EP300 (p300) mediated histone butyrylation is critical for adipogenesis

Aditya Bhattacharya [1], Sourav Chatterjee [1], Utsa Bhaduri [2], Akash Kumar Singh [1], Madavan Vasudevan [3], Koneni V Sashidhara [5], Rajdeep Guha [6], Aamir Nazir [7], Srikanta Kumar Rath [7], Nagashayana Natesh [8], Tapas K Kundu [1,4]

1 Transcription and Disease Laboratory, Molecular Biology and Genetics Unit, Jawaharlal Nehru Centre for Advanced Scientific Research, Bangalore, India.
2 Chromatin Biology Laboratory, Molecular Biology and Genetics Unit, Jawaharlal Nehru Centre for Advanced Scientific Research, Bangalore, India.
3 Theomics International Pvt Ltd, Bangalore
4 Division of Neuroscience and Aging Biology,CSIR-Central Drug Research Institute, Lucknow
5 Division of Medicinal and Process Chemistry, Central Drug Research Institute, Lucknow, India
6 Division of Laboratory Animal Facility, Central Drug Research Institute, Lucknow, India
7 Division of Toxicology and Experimental Medicine, Central Drug Research Institute, Lucknow, India
8 Central Government Health Scheme Wellness Centre Number 8, Domlur, Bangalore, India

E-mail ID of the corresponding author: tapas@jncasr.ac.in

Affiliations:

Aditya Bhattacharya – Ph.D. graduate student

Sourav Chatterjee – Post-doctoral researcher

Utsa Bhaduri – Research assistant

Madavan Vasudevan – Founder and CEO, Theomics International Pvt Ltd

Akash Kumar Singh - Integrated PhD student

Koneni V Sashidhara - Professor

Rajdeep Guha – Assistant Professor

Aamir Nazir- Principal Scientist

Srikanta Kumar Rath- Chief Scientist

Nagashayana Natesh – Senior physician

Tapas K Kundu - Professor

Abstract

Objective

The master epigenetic enzyme EP300 (p300) besides having lysine acetyltransferase activity can also catalyse other acylation modifications (propionylation, butyrylation, crotonylation etc.), the physiological implications of which are yet to be established fully. We hypothesized that p300 catalysed histone butyrylation may have a causal relationship with adipogenesis and the consequent obesity.

Methods

Histone butyrylation pattern was investigated in 3T3L1 cells upon adipogenesis by immunoblotting and chromatin immunoprecipitation experiments. A small molecule modulator that could specifically inhibit p300 catalysed butyrylation without affecting its canonical acetyltransferase activity was screened from a series of compounds and then administered in differentiating 3T3L1 adipocytes as well as high fat diet-induced and genetically obese mice to validate the importance of butyrylation in adipogenesis.

Results

Histone butyrylation was increased upon adipogenesis both globally and locally in the promoters of pro-adipogenic genes along with an upregulation in the expression of acyl CoA generating enzyme Acss2, knockdown of which led to reduced butyrylation. Treatment of differentiating 3T3L1 cells with the p300 specific butyrylation inhibitor LTK-14A led to

abrogation of adipogenesis with reduced expression of pro-adipogenic genes and inhibition of H4K5 butyrylation. LTK-14A administration could also attenuate weight gain in both mice models of obesity by preventing adipocyte hypertrophy via H4K5 butyrylation inhibition.

Conclusion

Our results indicate that p300 catalysed histone butyrylation may have a causal relationship with the process of adipogenesis. Site specific inhibition of butyrylation could lead to adipogenesis repression and hence this epigenetic modification could be targeted for obesity treatment.

Keywords: Acetylation; adipogenesis; butyrylation; garcinol; p300

Highlights

- Histone butyrylation has been established as a new epigenetic signature in the context of adipogenesis.
- To the best of our knowledge, this is the first report of a selective inhibitor of p300 catalysed histone acylation (butyrylation) without affecting its canonical acetyltransferase activity.
- Specific inhibition of H4K5 butyrylation could be a possible mechanism for inhibiting adipogenesis and hepatic steatosis leading to better control of obesity.
- LTK-14A class of molecule could be developed as anti-obesity therapeutics.

67 ## Introduction

68 Chromatin function is spatially and temporally regulated by several processes like incorporation of
69 histone variants, remodeling of nucleosomes by ATP-dependent remodelers and histone post-
70 translational modifications. Interestingly, epigenetics and the metabolic state of the cell are intimately
71 intertwined because the enzymes catalyzing the modifications use co-factors derived from several
72 metabolic reactions (1). In recent times, advancements made in high sensitivity mass spectrometry have
73 led to the discovery of new acylation modifications that structurally resemble acetylation, but differ in
74 hydrocarbon chain length, hydrophobicity and charge (2). Emerging evidence indicates that these
75 modifications occur dynamically on histones and could either have distinct functions from acetylation,
76 or, have a similar but more profound impact on chromatin de-compaction, thereby amplifying the
77 transcriptional output (3). EP300 (p300) is the master acyltransferase that has been found to
78 promiscuously acylate histones using diverse CoA derivatives (2).

79 Due to the rising prevalence of obesity in the modern-day society, there has been increased research on
80 the molecular mechanisms behind its manifestation. At the core of obesity lies the adipose tissue which
81 regulates energy homeostasis and metabolism. Hence, the developmental process of adipose tissue i.e.
82 adipogenesis and its dysregulation needs to be studied for clinical management of obesity-related
83 disorders. The process of adipogenesis is accompanied by a significant increase in global histone
84 acetylation levels, along with a rise in expression of p300 and a concomitant decrease in the levels of
85 several histone deacetylases (4). Regulation of gene expression is dictated by the fluctuating activities of
86 histone acetyltransferases and histone deacetylases. Moreover, the importance of histone acetylation
87 for adipogenesis has been further underlined by the finding that knockdown of ATP citrate lyase, an
88 enzyme responsible for the regeneration of acetyl CoA in the cytoplasm and nucleus, leads to decrease
89 in histone acetylation and also suppression of adipogenesis (5). Therefore, it can be assumed that p300

90 plays a crucial role in promoting the expression of adipogenesis related genes by acetylating the
91 histones in the corresponding gene regulatory regions, especially the promoters. Amongst the different
92 coenzyme A derivatives, butyric acid is an important short chain fatty acid and an intermediate of fatty
93 acid synthesis/breakdown processes. p300 has been known to carry out butyrylation of histones which
94 has been causally linked to the process of spermatogenesis (3).

95 In this study we report that histone butyrylation is critical in adipoogenesis, probed by the first known
96 acylation-specific small molecule inhibitor of p300. The newly discovered importance of histone
97 butyrylation in adipogenesis makes it an attractive target for small molecule compound mediated
98 inhibition of adipogenesis, thereby controlling obesity with lesser collateral damage.

99 **Materials and Methods**

100 **Animals and treatment for obesity-related studies:** Male C57BL/6J mice (8 weeks old) were bred in -
101 house and acclimatized for 1 week prior to experiments. Mice were maintained on a 12 hour light/dark
102 cycle and given ad libitum access to food and water. Experiments were carried out in accordance with
103 the Committee for the Purpose of Control and Supervision of Experiments on Animals (CPCSEA)
104 guidelines and were approved by the Institutional Animal Ethics Committee of JNCASR
105 (201/GO/Re/S/2000/CPCSEA dated 1st June, 2000 Renewed in Aug 2015). The age-matched animals
106 were maintained on a standard laboratory chow diet (AMRUT M/s Krishna Valley Agrotech ,
107 Maharashtra) or high fat diet (60 kcal% fat) (Research Diets, Cat. No. D12492) with or without LTK-14A
108 (50 mg/Kg body weight) and water. The compound was mixed with the high fat diet according to dosage
109 requirements in the laboratory every week. Body weight and food intake were measured twice every
110 week.

111 For the experiment on genetically obese mice, male db/db mice and db+/- mice (8-10 weeks old) bred
112 in-house were obtained and acclimatized for 1 week prior to experiments. Mice were maintained on a

113 12-hour light/dark cycle at 22+/-3 °C and a relative humidity of 55% and given ad libitum access to food
114 and water. The experiments were carried out in accordance with the Committee for the Purpose of
115 Control and Supervision of Experiments on Animals (CPCSEA) guidelines, Government of India and were
116 approved by the Institutional Animal Ethics Committee of CSIR-CDRI, Lucknow (IAEC/2020/115/Renew-
117 0/Sl.No.09). The age-matched animals were maintained on a standard laboratory pelleted diet (Altromin
118 International, Cat. No. 1320) and water. db/db mice were oral gavaged (50 mg/kg) with LTK14A in 0.5%
119 carboxymethyl cellulose, an equal volume of the vehicle was orally gavaged to control db/db mice for a
120 total period of 30 days. db+/- animals were kept as an untreated normal control group. The body
121 weights and feed intake was recorded every week throughout the experimental period.
122
123 **Cell culture:** The mammalian cell line 3T3L1 was obtained from ATCC (American Type Culture Collection)
124 and was grown in DMEM (Dulbecco's Modified Eagle's Medium). The growth medium was
125 supplemented with 10% FBS (Fetal Bovine Serum). The cell line was grown in 37°C incubator with 5%
126 CO2 and 90% relative humidity.
127
128 **Adipogenesis and Oil Red-O staining:** 3T3L1 preadipocytes were grown to confluency and 24 hours
129 post-confluence, cells were incubated with a differentiation medium (growth medium containing 1µM
130 Dexamethasone, 0.5 mM IBMX and 1 µg/ml insulin)(Sigma Aldrich) for 2 days in the presence/absence
131 of LTK-14A. Then the cells were supplemented with a maintenance medium with/without LTK-14A
132 (growth medium with 1 µg/ml insulin only) every alternate day. On the 6th day post-induction of
133 differentiation the cells were fixed with 3.7% formaldehyde solution followed by staining with Oil Red-O
134 dye (Sigma-Aldrich) (prepared in 60% isopropanol) for 1 hour at room temperature. The incorporated
135 dye was extracted using isopropanol and absorbance values were determined spectrophotometrically at
136 510 nm to estimate total amount of lipid accumulation under different experimental conditions.

137

138 **Acid extraction of histones and immunoblotting:** 3T3L1 cells were washed with ice-cold PBS and then
139 resuspended in Triton extraction buffer (PBS containing 0.5% Triton X-100 (v/v) and 2 mM PMSF). The
140 cells were allowed to lyse on ice for 10 minutes, spun down, washed with PBS and the process was
141 repeated another time. Then the proteins were acid extracted with 0.2 N HCl for two hours on ice. The
142 debris was spun down and then histones were precipitated by incubating the supernatant with 33%
143 trichloroacetic acid (Sigma-Aldrich) at 4°C for 30 minutes. The histones were then pelleted down and
144 then given two washes with acetone. The pellet was allowed to air-dry for 10 minutes and then
145 resuspended with 50 mM Tris-Cl, pH 7.4. Extraction of histones from epididymal fat pads was
146 performed by mechanically homogenizing the adipose tissues in Triton extraction buffer and then
147 following the same subsequent steps as mentioned before, except for the step of acid extraction with
148 HCl, in which the incubation was performed for four hours on ice.

149 The samples were then run in 15% SDS-PAGE, transferred onto PVDF membrane (Milipore) in transfer
150 buffer (25 mM Tris, 192 mM glycine, 0.036% SDS in 20% methanol), blocked with 5% skimmed milk
151 solution to prevent non-specific antibody binding and finally probed with antibodies against acetylation
152 and butyrylation marks prepared in 1% skimmed milk or FBS solution (5% BSA, 1x TBS, 0.1% Tween-20).
153 HRP-conjugated secondary antibodies (Abcam) were used against the primary antibodies to obtain a
154 chemiluminiscent signal in the presence of SuperSignal West Pico Chemiluminiscent Substrate (Thermo
155 Scientific) which was developed using the VersaDoc imaging system (Biorad).

156

157 **Synthesis of LTK14A:** Isolation of garcinol from Garcinia indica and synthesis of isogarcinol from it were
158 carried out following the protocols as mentioned in Mantelingu et al, (2007) (11). For LTK-14A synthesis,
159 anhydrous potassium carbonate (0.41 mmol) was added to a stirred solution of isogarcinol (100 mg, 0.16

160 mmol) in dry acetone. The mixture was stirred for 1 hour at room temperature followed by dropwise
161 addition of dimethyl sulfate (0.41 mmol) under a nitrogen gas atmosphere. The resulting reaction
162 mixture was further stirred at room temperature for 14 hours. Progress of the reaction was monitored
163 through thin layer chromatography. Acetone was evaporated from the reaction mass, ice was added and
164 acidified with 5% aqueous HCl (pH ~ 5-6). A pale brown precipitate was observed, which was filtered and
165 washed with cold water. The dry mass was then chromatographed on silica gel using 5-6% ethyl acetate
166 in hexane as an eluting solvent mixture. 720 mg (69%) LTK14A was isolated as a white solid. NMR
167 spectral analysis was consistent with the desired product (Sup. Fig.3A). A 20 mg sample was dissolved in
168 hot methanol and placed in a flat surface glass vial with access to very slow solvent evaporation. Crystals
169 as colorless needles were isolated. The purity of the synthesized LTK-14A was found to be more than
170 98% as verified by HPLC (Sup. Fig. 3C) and only the protonated species of LTK-14A were observed in the
171 ESI spectra of the corresponding fraction (Sup. Fig. 3B).

172

173 **X-ray crystal structure determination for LTK14A (CCDC: 1969185):** Suitable single crystal with
174 approximate dimensions of 0.35 × 0.18 × 0.15 mm3 was used for X-ray diffraction analyses by mounting
175 on the tip of a glass fibre in air. Data were collected on a Bruker kappa apex 2 with Mo Kα (λ=0.71073 Å)
176 at 296 (2) K. The structure was solved by direct method using program SHELXL-97 and subsequent Fast
177 Fourier Transform technique. Crystallographic data and experimental details for LTK14A are summarized
178 in Table 1 and Sup. Fig. 3D.

179

180 **Chromatin Immunoprecipitation:** Nuclear ChIP was performed using intact nuclei from cells after
181 removal of lipids. 3T3L1 that were either undifferentiated or differentiated for 3 to 6 days were cross-
182 linked using 1% formaldehyde. Nuclear fractions were obtained by sequentially lysing the cells in two

183 buffers- lysis buffer 1 (140 mM NaCl, 1 mM EDTA, 50 mM HEPES, 10% Glycerol, 0.5% NP-40, 0.25%
184 Triton X-100) and lysis buffer 2 (10 mM Tris pH 8, 200 mM NaCl, 1 mM EDTA, 0.5 mM EGTA). This was
185 followed by lysis in SDS lysis buffer (1% SDS, 10 mM EDTA, 50 mM Tris-HCl pH 8). Lysates were sonicated
186 in a Diagenode Bioruptor (Liège, Belgium) to produce 200 to 1000 bp DNA fragments. The cell lysates
187 were incubated with H4K5 Bu antibody (PTM Biolabs) or preimmune IgG per sample and 25 µl of
188 magnetic protein G Dynabeads (catalog no. 10003D; Novex, Waltham, MA) overnight at 4°C. Beads were
189 then washed successively with low-salt buffer (0.1% SDS, 1% Triton X-100, 2 mM EDTA, 20 mM Tris-HCl
190 pH 8, and 150 mM NaCl), high-salt buffer (0.1% SDS, 1% Triton X-100, 2 mM EDTA, 20 mM Tris-HCl pH 8,
191 and 500 mM NaCl), LiCl buffer (250 mM LiCl, 1% NP-40, 1% NaDOC, 1 mM EDTA, and 10 mM Tris-HCl, pH
192 8), and TE (10 mM Tris-HCl pH 8 and 1 mM EDTA). DNA-protein complexes were recovered from beads
193 in elution buffer (0.1% SDS and 100 mM NaHCO3). The ChIP eluates and input samples in the elution
194 buffer were then reverse cross-linked by adding 200 mM NaCl and 20 µg proteinase K (Sigma) and
195 incubating at 65°C for 4 h. Subsequently, 20 µg of RNase A (Sigma) were added and the samples were
196 further incubated for 15 min at 37°C. The immunoprecipitated DNA was extracted using phenol-
197 chloroform, ethanol precipitated, and used for quantitative PCR. The region-specific primer sets used for
198 the ChIP-qPCR analysis have been mentioned in Table 3. These primers were designed based on the
199 genomic coordinates with enriched H3K27 acetylation in the vicinity of promoters of candidate genes in
200 brown adipose tissue, the information for which was obtained from NCBI37/mm9 assembly
201 (ENCODE/LICR).

202

203 **Immunohistochemistry:** Collected liver tissue samples were stored in 4% paraformaldehyde for 24
204 hours after which they were cryoprotected in 30% sucrose solution for two weeks. Cryosections were
205 performed at 7 µm sections using Cryostat LeicaCM1850 UV. For staining, the tissue sections were

206 washed with PBS followed by antigen retrieval with 0.01 M citrate buffer (pH 6). The tissues were then
207 permeabilised with 0.3% Triton X-100/PBS (PBST) and blocked with 2% serum followed by incubation
208 with primary antibodies overnight at 4°C. The next day, secondary antibody incubation was carried out
209 for one hour at room temperature followed by staining of the nuclei with Hoechst 33342 and mounting
210 with 70% glycerol. Images were acquired by confocal microscopy. For quantitation, the intensity of each
211 modification-specific staining was normalized with respect to the Hoechst staining intensity.

212

213 **Reagents and antibodies:** The media used for cell culture was purchased from Sigma-Aldrich; DMEM
214 (Ref: 1152). Several other cell culture reagents were obtained from HIMEDIA, such as PBS (Ref: TL1006),
215 Trypsin-EDTA solution 10X (Ref: TCL070) and Antibiotic antimyotic solution 100X (Ref: A002A). Multiple
216 reagents used for cell culture were obtained from Sigma-Aldrich: Insulin (Ref: I6634), Dexamethasone
217 (Ref: D4902), IBMX (Ref: I5879). TRIzol reagent was obtained from Ambion life technologies (Ref:
218 15596018). The commercial antibodies used in this study are Pan anti-butyryllysine (PTM Biolabs, SKU:
219 PTM 301), Butyryl-Histone H4 (Lys 12) rabbit pAb (PTM Biolabs, SKU: PTM 308), Butyryl-Histone H3 (Lys
220 9) rabbit pAb (PTM Biolabs, SKU: PTM 305), Butyryl-Histone H3 (Lys 23) mouse mAb (PTM Biolabs, SKU:
221 PTM 307), Butyryl-Histone H4 (Lys 8) rabbit pAb (PTM Biolabs, SKU: PTM 311), Butyryl-Histone H4 (Lys 5)
222 rabbit pAb (PTM Biolabs, SKU: PTM 313), Butyryl-Histone H3 (Lys 27) rabbit pAb (PTM Biolabs, SKU: PTM
223 315).

224 **Statistical analysis:** All statistical analyses were performed using GraphPad Prism 7 Software (California,
225 USA). Data obtained from two or three individual experiments as mentioned in figure legends, were
226 expressed as mean +/- SD. Either two-tailed unpaired Student's t-test or one-way ANOVA with
227 Dunnett's/Bonferroni's multiple comparision was used to determine the statistical significance values.

228 The mutagenecity analysis data were analyzed by comparing the groups using one-way ANOVA followed
229 by Neman-Keuls test. Body weight data for acute toxicity test were summarized in Mean ± SD and
230 compared by two factor (Group and Period) repeated measure analysis of variance (RM ANOVA) and the
231 significance of mean difference within (intra) and between (inter) the groups was done by Newman-
232 Keuls post hoc test. A P-value of equal to or less than 0.05 was considered statistically significant.

233 **Acknowledgements:** TKK is a recipient of JC Bose fellowship from the Department of Science and
234 Technology, Govt. of India (SR/S2/JCB-28/2010). AB is a senior research fellow of UGC. This work was
235 supported by Life Science Education & Training at JNCASR grant (DBT/INF/22/SP27679/2018). We
236 acknowledge Dr. Rahul Gajbhiye from NIPER, Kolkata for the assistance in mass spectrometry-related
237 experiments in their central instrument facility. We thank Dr. R.G. Prakash for providing the necessary
238 facilities to perform the mice experiment in Animal Facility, JNCASR and the confocal facility, JNCASR for
239 the immunofluorescence imaging analysis. We also thank Kruthi HT for helping in the preparation of the
240 figures and graphical abstract. We further acknowledge the Sophisticated Analytical Instrument Facility
241 and Research (SAIFR, Lucknow) for providing spectral data. This manuscript bears CDRI communication
242 number 2021/TK.

243

244 **Conflict of interest:** Authors declare no conflict of interest.

245 **Author Contributions:** AB and TKK conceived the project. AB designed and performed all the biological
246 experiments. SC performed the initial synthesis of all compounds and molecular docking analysis. KVS
247 performed bulk scale synthesis of LTK-14A for animal experiments. AKS and RG assisted in the animal
248 experiments. UB and MV performed *in silico* analysis of high throughput RNA sequencing data. AN did
249 the toxicity evaluation and SKR evaluated the mutagenecity. NN provided the raw material *Garcinia*
250 *indica* for compound isolation. AB and TKK analyzed the data and wrote the manuscript.

251 **Results**

252 **Physiological levels of butyryl CoA and histone butyrylation increase during adipogenesis:**

253 Under normal circumstances, the cellular levels of specific coenzyme A derivatives are much less than
254 acetyl CoA (6).We surmised that the situation might alter in particular cases where metabolic pathways
255 promoting the production of other acyl CoA derivatives become more predominant. One such possible
256 scenario could be the process of adipogenesis in which fatty acid synthesis and breakdown can give rise
257 to several intermediate products like butyryl CoA.

258 The causal relationship between butyryl CoA and adipogenesis was investigated using the 3T3L1 pre-
259 adipocyte cell line as a model system (fig 1A). Our RT-qPCR data showed a significant increase in the
260 expression of *Acss2* (acyl-CoA synthetase short-chain family member 2) upon differentiation (fig 1B).
261 Previously, ACSS2 had been established as the enzyme responsible for the generation of acyl-CoA
262 derivatives from their corresponding short chain fatty acids (7). Indeed, siRNA mediated knockdown of
263 *Acss2* (fig 1C) led to a drastic reduction in histone butyrylation with a relatively lesser effect on
264 acetylation (fig 1D). This indicated that the ACSS2 generated butyryl CoA might be playing an important
265 physiological role in adipogenesis. These findings prompted us to investigate whether adipocyte
266 differentiation also led to an increased butyrylation of proteins. We observed that in accordance with
267 the previous report (4), there was an increase in acetylation level at histone H3 lysine 9 (H3K9 Ac) in the
268 differentiated cells as compared to the undifferentiated cells (Fig. 1C, panel i). Interestingly
269 immunoblotting with pan butyryllysine and site-specific antibodies (H3K9, H3K23, H3K27, H4K5, H4K8
270 and H4K12) against butyrylation (Fig 1C, panel ii and iii) revealed that butyrylation at each of these sites
271 also increased upon differentiation. Chromatin immunoprecipitation with antibody against H4K5
272 butyrylation revealed that the modification enrichment levels increased in promoters of different pro-
273 adipogenic genes in a time dependant manner. *Pparg*, the master regulator of adipogenesis, exhibited a

274 steady increase in butyrylation level in its promoter with the progress of differentiation (fig 1F, panel i)
275 while butyrylation increased only at the terminal stage of adipogenesis in the promoter of *Lep*, encoding
276 the adipocyte marker leptin which gets expressed in mature adipocytes (fig 1F, panel ii). Interestingly,
277 the promoter of *Cebpd*, which regulates *Pparg* expression did not show any enhanced butyrylation in its
278 promoter on day 3 and instead, exhibited increased butyrylation on day 6 of adipogenesis (fig 1F, panel
279 iii). Collectively these results showed that during adipogenesis, EP300 catalysed butyrylation of
280 histones could be an important epigenetic signature.

281

282 **Identification of a small molecule that selectively inhibits p300 catalysed histone butyrylation *in vitro*:**

283 In order to investigate the contribution of p300 catalyzed butyrylation per se in adipogenesis, we
284 adopted a chemical biology-based approach. For this purpose, a series of derivatives of garcinol, a
285 polyisoprenylated benzophenone isolated from *Garcinia indica*, were synthesized (8). These derivatives,
286 unlike garcinol, were found to be non-toxic to cells and showed a high specificity toward the catalytic
287 activity inhibition of EP300. The derivatives were generated by internal cyclisation of garcinol with
288 further addition of one or two functional groups to the remaining free -OH groups- giving rise to mono
289 and disubstituted derivatives (Sup. fig. 1A). Amongst these, a few monosubstituted derivatives could
290 potently inhibit EP300 catalysed acetylation as well as butyrylation, while their disubstituted
291 counterparts were unable to inhibit acetylation (Sup. fig. 2 B, C and D). This was probably due to
292 increased steric hindrance brought about by the addition of an extra functional group that interfered
293 with the interaction between the compounds and EP300.

294 An inverse correlation between catalytic rates of acylation reactions by EP300 and increasing acyl chain
295 length had already been established previously (9). Based on this, we hypothesized since butyrylation is
296 catalysed by EP300 at a much slower rate than acetylation, one of the compounds that could not inhibit

297 EP300 catalysed acetylation might be able to inhibit the slower butyrylation reaction. Our *in vitro*
298 butyrylation assay using recombinant p300 and histone H3 as the substrate revealed a few potential
299 candidates (Sup. Fig. 2 E) as butyrylation inhibitors. Amongst them, LTK-14A, which is 13, 14 dimethoxy
300 isogarcinol, was capable of inhibiting full-length EP300 catalysed butyrylation at a concentration of 25
301 µM (fig. 2 C and D), with minimal effect on EP300 catalysed acetylation in similar reaction conditions (fig.
302 2 A and B).

303 In order to understand the underlying mechanism of the selective inhibition by LTK-14A, we performed
304 molecular docking analysis of LTK-14A (Fig. 2 G) and the catalytic domain. To delineate this, we solved
305 the crystal structure of LTK-14A (Table 1, Sup. Fig.2A). LTK-14 (fig. 2E), a specific inhibitor of EP300
306 catalysed acetylation and butyrylation (Sup. Fig. 2 B and C) was used for further comparative analysis.
307 The energy minimized analysis revealed that both LTK-14 and LTK-14A could potentially bind with the
308 active site of the EP300 catalytic domain forming several hydrophobic interactions (Fig.2 F and H). LTK-
309 14, due to the presence of a free phenolic –OH group, could hydrogen bond with a carbonyl oxygen
310 atom present in the peptide backbone of S1396 residue. However, LTK-14A has all of its phenolic –OH
311 groups blocked and so it is incapable of forming such an interaction. This hydrogen bonding by LTK-14
312 could imply a stronger binding to the enzyme, while LTK-14A, by interacting with fewer residues
313 presumably inhibits only the slower butyrylation reaction and the interaction may not be strong enough
314 to deter the faster acetylation reaction.

315 Some of the residues with which LTK-14A could potentially form hydrophobic interaction have already
316 been reported before as being critical for targeting inhibition of the enzymatic activity of EP300 by the
317 first reported EP300 inhibitor lysyl CoA (10). These residues include C1438, Y1446, Y1397 and W1436. To
318 verify this observation we generated a point mutant of p300 catalytic domain in which cysteine 1438,
319 showing the highest propensity to interact with LTK-14A, was mutated to alanine. We found that the

320 C1438A catalytic domain is equally active as the wild-type catalytic domain in an *in vitro* lysine
321 acetyltransferase assay (Sup. Fig. 2B). We observed that the wild-type EP300 catalytic domain catalysed
322 butyrylation was inhibited by LTK-14A most prominently at 25 µM concentration while acetylation was
323 not inhibited (compare lane 6 in each of fig.2 I-L). In contrast, neither acetylation nor butyrylation
324 modification catalysed by the mutant EP300 catalytic domain could be inhibited by LTK-14A even at 25
325 µM concentration (compare lane 6 in each of fig. 2 M-P). Altogether, these data suggest that LTK-14A
326 indeed interacts with C1438 within the active site of the EP300 catalytic domain, and this residue is
327 critical for its interaction to bring about butyrylation reaction inhibition.

328 **LTK-14A is a metabolically stable, cell-permeable compound that significantly inhibits adipogenesis:**

329 Upon establishing that LTK-14A is an EP300 acylation-specific inhibitor *in vitro*, its cellular effects were
330 tested using 3T3L1 cells. The quality of our compound used in all biological experiments was acceptably
331 good with more than 97% purity (Sup. Fig. 2 C, D and E). We found the LTK14A is highly cell-permeable
332 and metabolically stable as it could be detected by mass spectrometry analysis from metabolites
333 extracted from LTK-14A treated cells after six days (Fig. 3A). MTT assay showed that LTK-14A at 25 µM
334 concentration did not have any adverse effect on the cellular oxidoreductase activity, a signature of
335 metabolic output of cells, (Fig. 3B) suggesting that LTK-14A is non-toxic to 3T3L1 even after 6 days of
336 treatment. Oil Red-O staining of 3T3L1 cells differentiated in the presence of LTK-14A followed by
337 spectrophotometric quantitaion revealed significant inhibition of adipogenesis by the compound (Fig.
338 3C, D).

339 In order to understand the transcriptional mechanism of LTK14A-mediated butyrylation inhibition on
340 adipogenesis, adipogenic cells were treated with LTK-14A and subjected to transcriptome analysis. We
341 used untreated and solvent treated cells as control. Volcano plot (Fig. 3E) and heat map analysis (Fig. 3F)
342 revealed that upon treatment with the compound, a large number of genes were differentially

343 expressed compared to DMSO treated and untreated conditions. To better understand the LTK-14A
344 affected genes, we focused on the common genes that were differentially expressed in the two cases-
345 (1) LTK-14A versus no inhibitor and (2) LTK-14A versus DMSO. Among these common genes, 2200 genes
346 were found to be downregulated and 1309 genes were upregulated (Fig. 4A) with a majority of them to
347 be protein-coding genes (Fig. 4B). Gene ontology analysis revealed that LTK14A treatment
348 predominantly affected the genes involved in lipid metabolism pathways (Fig. 4C, E) which were
349 minimally affected by DMSO alone (Fig. 4D). The gene regulatory networks and the respective pathways
350 were constructed with the major genes that were affected by LTK-14A treatment compared to DMSO
351 treated and untreated conditions (Fig. 4F, Sup. Fig.3A). They collectively depict how LTK-14A, by
352 inhibiting the expression of a large number of genes that are interconnected via several pathways
353 associated with lipid metabolism, brings about a collapse in the adipogenesis process as a whole.

354 A few of the pro-adipogenic genes downregulated by LTK-14A, as indicated by RNA sequencing, were
355 selected for further validation (Sup. Fig. 3B). RT-qPCR analysis corroborated that except for *Cebpd*, most
356 of the other pro-adipogenic genes (*Pparg, Cebpa, Adipoq, Lep, Slc2a4, Fasn* and *Fabp4*) showed a
357 marked downregulation upon LTK-14A treatment (Fig. 4G). *Acss2* was also downregulated by LTK-14A
358 (Sup. Fig.4C). The upregulation of anti-adipogenic genes was also verified by performing RT-qPCR
359 analysis for two such candidate genes- *Kdm4c* and *Tead4* (Sup. Fig.3C). Collectively, the RNA sequencing
360 analysis and the validation of gene targets further convincingly suggested that LTK-14A can inhibit
361 adipogenesis in 3T3L1 cells, mainly by repressing the expression of important pro-adipogenic genes.

362

363 **LTK-14A inhibits histone butyrylation in 3T3L1 cells, without affecting acetylation or other post-**
364 **translational modifications:**

365 Furthermore we wanted to find out whether LTK-14A mediated downregulation of adipogenesis is
366 causally linked to the inhibition of histone butyrylation in the 3T3L1 cells. We observed that treatment
367 with LTK-14A inhibited overall butyrylation of histones (Fig. 5 A, B). Among the specific modification sites
368 tested, H3K23 and H4K5 butyrylation showed a significant decrease upon treatment with LTK-14A (Fig. 5
369 A, B) while butyrylation at other tested sites was affected minimally (Sup. Fig. 3D). Acetylation of
370 histones (H3K9, H3K18 and H4K12) was also found to be unaffected (Fig. 5 C, D) upon LTK-14A
371 treatment. To establish the specificity of the LTK14A, the effect of LTK-14A on lysine and arginine
372 methylation along with phosphorylation of histones was also investigated. We observed (Fig. 5 E, F) no
373 significant changes in these marks upon the compound treatment, thereby indicating that in the 3T3L1
374 cells, LTK-14A specifically inhibits butyrylation.

375

376 **Inhibition of butyrylation attenuates weight gain of high fat diet fed C57BL6/J mice:**

377 After observing the anti-adipogenic effect of LTK-14A on 3T3L1 cells, we investigated whether this
378 compound could also affect adipogenesis and obesity at an organismal level. For this purpose, C57BL6/J
379 mice were maintained either on a normal diet or a high fat diet with or without LTK-14A. In due course
380 of time it was observed that the mice maintained on a high fat diet along with LTK-14A had a weight
381 gaining trend intermediate between the normal diet and high fat diet fed mice (Fig.6A,B). Dissection of
382 the mice revealed that the fat accumulation in high fat diet-fed mice was the highest, followed by those
383 on high fat diet and LTK-14A, and then by those on normal diet (Fig. 6C). The epididymal fat pads were
384 separately weighed and again it was observed that the weights of the fat pads from compound treated
385 mice were much less than that of high fat diet-fed mice (Fig. 6 D, E). The diet consumption pattern of the
386 mice showed that the two groups on high fat diet with or without LTK-14A, had a similar consumption
387 rate indicating that the reduced weight gain of the compound treated mice is not due to discrepancy in

388 diet consumption (Table 2). Hematoxylin and eosin staining of adipose tissue and liver (Fig. 6 F,G)
389 showed signs of adipocyte hypertrophy and hepatic steatosis in high fat diet-fed mice, which were
390 absent in the mice maintained on normal diet or high fat diet with LTK-14A.

391 Immunofluorescence staining of the liver tissue samples revealed that there was a significant increase in
392 H4K5 butyrylation levels in high fat diet-fed mice compared to normal diet-fed mice in which the
393 modification was barely detectable and it was almost completely inhibited upon LTK-14A treatment (Fig.
394 6H panel iii, Fig. 6I panel iii). On the other hand, no significant difference in H4K12 (Fig. 6H panel i, Fig. 6I
395 panel i) and H3K14 acetylation (Fig. 6H panel ii, Fig. 6I panel ii) levels could be observed across all the
396 three groups. Furthermore, histone modification pattern in the adipose tissues was studied with acid
397 extracted histones from the epididymal fat pads. H4K5 butyrylation was reduced in the LTK-14A treated
398 samples compared to those of high fat diet-fed mice (Fig. 6 J, N) while H3K14, H3K18 and H4K12
399 acetylation levels were relatively unchanged across all the three groups (Fig. 6 J, K, L, M). The metabolic
400 stability of LTK-14A in mice was verified by its detection in ESI spectra of analytes extracted from the
401 liver of compound treated mice (Sup. Fig 3 E).

402 **The butyrylation specific inhibitor reduces the weight of genetically obese db/db mice:**

403 The previous model system involved the use of LTK-14A as a prophylactic. To test whether LTK-14A
404 could also reduce obesity by inhibiting histone butyrylation, genetically obese homozygous mutant
405 db/db mice were used. Heterozygous mutant db+/- mice were taken as control. The hyperphagic db/db
406 mice were orally administered LTK-14A daily at the same dosage as before (50 mg/Kg body weight). We
407 observed that upon oral gavaging of LTK-14A, the overweight mice not only showed an arrest in weight
408 gain, but their body weights were significantly reduced by the end of one month of treatment (Fig. 7 A,
409 B, C). The food intake of LTK-14A treated mice was marginally less than that of the vehicle-treated mice
410 (Table 2, Supplementary Information), although both groups consumed more food compared to the

411 db+/- mice during the treatment regime. The average weight of the liver (Fig. 7 D,E) and epididymal fat
412 pads (Fig. 7 F,G) was the highest for db/db mice given vehicle control and least for the db+/- mice, while
413 that for the compound treated db/db mice was intermediate. Hematoxylin and eosin staining of liver
414 and adipose tissue(Fig. 7 H,I) showed signs of adipocyte hypertrophy and hepatocyte ballooning in
415 vehicle-treated db/db mice, which were absent in the db+/- and LTK-14A treated db/db mice.

416 Similar to the high fat diet-induced obesity model, the more obese homozygous leptin receptor mutant
417 mice (db/db) liver had a greater level of H4K5 butyrylation compared to leaner heterozygous mutant
418 mice (db +/-) (Fig 7J panel iii, Fig. 7K panel iii). Moreover, LTK-14A treated db/db mice liver showed a
419 decrease in H4K5 butyrylation compared to vehicle control-treated mice liver. In contrast, H4K12 (Fig. 7J
420 panel i, Fig. 7K panel i) and H3K14 acetylation (Fig. 7J panel ii, Fig. 7K panel ii) were only partially
421 upregulated in the db/db mice and did not get significantly reduced upon LTK-14A treatment.
422 Immunoblotting with acid extracted histones from epididymal fat pads showed that H4K5 butyrylation
423 was reduced in the adipose tissues of LTK-14A treated mice (Fig. 7 L,P) compared to vehicle control
424 treated obese mice. H3K14, H3K18 and H4K12 acetylation were not significantly altered in any of the
425 three groups (Fig. 7 L,M,N,O). Finally, RT-qPCR analysis showed that just like in cellular model of
426 adipogenesis, LTK-14A treatment led to robust inhibition of important pro-adipogenic genes *Pparg*, *Lep*,
427 *Slc2a4* and *Adipoq* in the fat pads of compound treated db/db mice (Fig. 7Q). Collectively these data
428 establish that obesity can not only be prevented but also reverted by specific inhibition of H4K5
429 butyrylation, thereby highlighting the importance of this modification in the context of adipogenesis.

430 **LTK-14A is non-mutagenic and non-toxic in nature for biological applications:** Based on the
431 observations of obesity attenuating effects of LTK-14A in two different mice models, we performed
432 some preclinical tests to ensure that the obesity arrest was not a result of any deleterious side effect of
433 toxicity from the compound. Plate incorporation assay was carried out in four different nutritional

434 auxotrophic mutants of Salmonella typhimurium (TA97a, TA98, TA100 & TA102) in the absence or
435 presence of rat liver extract (S9 enzyme fraction). It was observed that the number of revertants
436 obtained from LTK-14A was similar to that from vehicle control and far less compared to that from the
437 positive control in all four strains, both in the absence and presence of liver extract (Sup. Fig 4 A-H).
438 Furthermore, acute toxicity test was performed on rats for checking whether a single administration of
439 excessively high dose of LTK-14A would alter the body weight and food/water consumption pattern of
440 the rats. The body weight changes in the LTK-14A administered rats were similar to the vehicle control-
441 treated ones (Table 6) with no gross morphological changes in any organ. Moreover, there was also no
442 significant treatment-related effect on the food and water consumption of rats of both gender for all
443 three doses compared to vehicle control (Table 6).

444 Collectively these data imply that LTK-14A does not have deleterious toxic effects on the test animals
445 and could have a potential for downstream applications for tackling obesity-related complications.

446

447

448

449

450 **Discussion**

451 Reports on the physiological relevance of acylation modifications are scanty. Breakthroughs have been
452 made in establishing the importance of butyrylation in spermatogenesis (5), β-hydroxybutyrylation in
453 starvation response (11) and crotonylation in inflammatory response, digestive system, cancer and HIV
454 latency (7,12,13,14). Lysine propionylation has also been reported as an activation mark on histones
455 that could be useful in various physiological processes (15). The list of these modifications seems to be

456 increasing continuously, with the recent additions of histone serotonylation (16), lactylation (17) and
457 dopaminylation (18). The fact that serotonin and dopamine are chemical neurotransmitters while
458 lactate is derived from pyruvate, a glycolytic end product, and all these molecules bring about a
459 modification of histones thereby mediating gene expression in several tissues, bear testimony to the
460 hypothesis that the abundance levels of cellular metabolites in different physiological contexts can lead
461 to modification of histones with a plethora of diverse chemical moieties that can selectively modulate
462 gene expression patterns.

463 Our initial experiments in 3T3L1 adipogenesis indicated an important role of ACSS2 in the differentiation
464 process by generating butyryl CoA for histone butyrylation. Inside the cells ACL (ATP citrate lyase) and
465 ACSS2 have been implicated in the generation of nuclear acetyl CoA. Both the enzymes are known for
466 regulating gene expression in different contexts by acetylating histones in specific genomic loci (19-21).
467 Knockdown of *Acss2* had a much more pronounced effect on H4K5 butyrylation compared to H3K18
468 acetylation. This is probably due to the fact that ACSS2 is the sole/major producer of acyl CoA species
469 while acetyl CoA can be generated by diverse means and the knockdown of a single acetyl CoA producer
470 was not enough to have a robust effect on global acetylation level of histones. Similar observations have
471 already been made for histone crotonylation in HeLa cells (7).

472 Due to redundancy in the functionality of p300 catalyzed butyrylation with acetylation, the significance
473 of butyrylation in adipogenesis was demonstrated using a pharmacological approach. LTK-14A could
474 selectively and specifically inhibit histone butyrylation and still inhibit adipogenesis by downregulating
475 the expression of many pro-adipogenic genes. However amongst these genes *CEBPd* expression did not
476 get affected by LTK-14A possibly because the expression of this gene is less prone to be regulated by
477 histone butyrylation in its promoter. Indeed, our chromatin immunoprecipitation study indicated that in
478 the initial stage of induction of differentiation in pre-adipocytes, there was no enrichment of H4K5

479 butyrylation in the promoter of *Cebpd*. This could explain why the butyrylation inhibitor LTK-14A
480 treatment at the induction stage did not inhibit *Cebpd* expression, since there was no buyrylation mark
481 enrichment for inhibition in its promoter to begin with. An increased butyrylation in its promoter at the
482 terminal stage could be either through p300 catalysed modification or non-enzymatic means with
483 greater availability of butyryl CoA, or both. Currently, we have not been able to verify this. However our
484 preliminary observations with promoter-specific studies indicate that H4K5 butyrylation plays a role in
485 regulating the expression of the critical transcription factor *Pparg*. Inhibition of butyrylation by LTK-14A
486 repressed the expression of the master regulator which further led to the inhibition of downstream
487 genes like *Lep*, whose expression is dependent on PPARγ. While cell line-based studies indicate that
488 C/EBPδ regulates the expression of a cascade of transcription factors like C/EBPα and PPARγ, this fact
489 has been questioned in knockout mice which have poorly differentiated adipose tissue but still express
490 *Pparg* and *Cebpa* (22). This indicates that there could be other factors playing a redundant function like
491 C/EBPδ in the initiation stage of adipogenesis. Moreover, an additional function of C/EBPδ may seem to
492 be downstream of C/EBPα and PPARγ at the terminal stage of adipogenesis. It has been speculated that
493 this could involve inducing the expression of ligands that activate PPARγ (23). Therefore, the increased
494 butyrylation in the promoter of *Cebpd* on day 6 of adipogenesis might be responsible for its role in the
495 terminal stage. The expression of *Cebpd* is independent of *Pparg* and hence repression of *Pparg* by
496 butyrylation inhibition with LTK-14A did not repress *Cebpd*.

497 *Acss2*, which encodes the enzyme responsible for butyryl CoA biosynthesis was also downregulated by
498 LTK-14A which might have further contributed to reduced butyrylation of histones during inhibition of
499 adipogenesis. Amongst the different histone modification patterns investigated, H4K5 butyrylation was
500 consistently affected by LTK-14A in different cell line and mice models, while the other site specific
501 butyrylation marks were relatively unaltered, indicating that there may be a hierarchy in the importance
502 of these modifications in the regulation of adipogenesis. While our work was in progress, a new report

503 was published in which it was demonstrated that inhibition of fatty acid synthesis as well as oxidation
504 leads to a reduction in H4K5 butyrylation while acetylation remains unaffected (24). This further
505 reinforces our own hypothesis that fatty acid metabolism is an important source for certain acyl CoAs
506 such as butyryl CoA, derived from the short chain fatty acid butyric acid. Another work published during
507 this period revealed that HBO1, a member of the MYST family of acetyltransferase, also possesses the
508 ability to catalyse acylation reactions including butyrylation (25). Mass spectrometry studies of histone
509 modifications altered by knockdown of HBO1 in HeLa cells showed that H4K5 butyrylation does not get
510 affected by depletion of HBO1 indicating that it is a p300 specific mark. LTK-14, the monomethoxy
511 derivative of isogarcinol was found to be a specific inhibitor of p300 acetyltransferase activity (8)
512 without affecting PCAF. Since its disubstituted counterpart LTK-14A was found to be relatively inert with
513 respect to LTK-14, it seems plausible that LTK-14A would be unlikely to affect other epigenetic
514 modifications besides p300 catalysed acylation.

515 Global histone acetylation has previously been reported to remain unchanged in liver and adipose
516 tissues of mice even after high fat diet consumption (26), which was consistent with the observations we
517 made in both mice models studied. Since acetyl CoA is highly abundant, fluctuations in its levels did not
518 lead to major changes in histone acetylation patterns. Because the usual butyryl CoA levels are far less
519 than their corresponding Michaelis Menten constant for p300, an increase in butyryl CoA levels due to
520 excess lipid consumption through high fat diet or *de novo* lipid synthesis through excess food
521 consumption, resulted in a concomitant increase in butyrylation by p300 which served as the nutritional
522 sensor for butyryl CoA. Enhanced H4K5 butyrylation was not observed in mature adipose tissues of
523 obese mice possibly due to the predominance of adipocyte population in the tissues of mice from all the
524 groups (27).

525

526 **Conclusion**

527 In the 21st century, obesity has become a major epidemic leading to several other disorders such as
528 type 2 diabetes and arteriosclerosis. Histone acetylation inhibition could be regarded as a possible
529 method for attenuating adipogenesis and obesity. But acetylation is a widespread phenomenon that is
530 required in several other physiological processes besides adipogenesis. Hence, treatment with an
531 acetyltransferase inhibitor at a particular range of concentration could have undesirable side effects and
532 toxicity. In contrast, butyrylation is a rarer event, repressing which may be less harmful to other
533 processes. Indeed, our preclinical tests are indicative of the fact that LTK-14A may be suitable for
534 development as a possible anti-obesity drug due to its negligible toxicity side effects. The present finding
535 thus establishes the importance of histone butyrylation in adipogenesis, making it an attractive target
536 for pharmacological inhibition of adipogenesis and thereby controlling obesity (Graphical abstract).

537 **References**

538 **1.** Haws, S. A., Leech, C. M., Denu, J. M. Metabolism and the Epigenome: A Dynamic Relationship.
539 Trends Biochem 2020; 45, 731-747

540 **2.** Chen, Y., Sprung, R., Tang, Y., Ball, H., Sangras, B., Kim et al Lysine propionylation and
541 butyrylation are novel post-translational modifications in histones. Mol Cell Proteomics 2007; **6**:
542 812-819

543 **3.** Goudarzi, A., Zhang, D., Huang, H., Barral, S., Kwon, O. K., Qi, S. et al Dynamic Competing
544 Histone H4 K5K8 Acetylation and Butyrylation Are Hallmarks of Highly Active Gene Promoters.
545 Mol Cell 2016;**62**:169-180

546 **4.** Yoo, E. J., Chung, J. J., Choe, S. S., Kim, K. H., and Kim, J. B. Down-regulation of histone
547 deacetylases stimulates adipocyte differentiation. J Biol Chem 2006; **281**:6608-6615

548 **5.** Wellen, K. E., Hatzivassiliou, G., Sachdeva, U. M., Bui, T. V., Cross, J. R., and Thompson, C. B. ATP-
549 citrate lyase links cellular metabolism to histone acetylation. Science 2009;**324**:1076-1080
550 **6.** King, M. T., and Reiss, P. D. Separation and measurement of short-chain coenzyme-A
551 compounds in rat liver by reversed-phase high-performance liquid chromatography. Anal
552 Biochem 1985;**146**:173-179
553 **7.** Sabari, B. R., Tang, Z., Huang, H., Yong-Gonzalez, V., Molina, H., Kong, H. E. et al Intracellular
554 crotonyl-CoA stimulates transcription through p300-catalyzed histone crotonylation. Mol Cell
555 2015;**58**:203-215
556 **8.** Mantelingu, K., Reddy, B. A., Swaminathan, V., Kishore, A. H., Siddappa, N. B., Kumar, G. V. et al
557 Specific inhibition of p300-HAT alters global gene expression and represses HIV replication.
558 Chem Biol 2007;**14**:645-657
559 **9.** Kaczmarska, Z., Ortega, E., Goudarzi, A., Huang, H., Kim, S., Márquez et al Structure of p300 in
560 complex with acyl-CoA variants. Nat Chem Biol 2017; **13**:21-29
561 **10.** Liu, X., Wang, L., Zhao, K., Thompson, P. R., Hwang, Y., Marmorstein, R. et al The structural basis
562 of protein acetylation by the p300/CBP transcriptional coactivator. Nature 2008;**451**:846-850
563 **11.** Xie, Z., Zhang, D., Chung, D., Tang, Z., Huang, H., Dai, L. et al Metabolic Regulation of Gene
564 Expression by Histone Lysine β-Hydroxybutyrylation. Mol Cell 2016;**62**:194-206
565 **12.** Fellows, R., Denizot, J., Stellato, C., Cuomo, A., Jain, P., Stoyanova, E. et al Microbiota derived
566 short chain fatty acids promote histone crotonylation in the colon through histone deacetylases.
567 Nat Commun 2018;**9**:105
568 **13.** Wan, J., Liu, H., and Ming, L. Lysine crotonylation is involved in hepatocellular carcinoma
569 progression. Biomed Pharmacother 2019;**111**:976-982
570 **14.** Jiang, G., Nguyen, D., Archin, N. M., Yukl, S. A., Méndez-Lagares, G., Tang, Y. et al HIV latency is
571 reversed by ACSS2-driven histone crotonylation. J Clin Invest 2018;**128**:1190-1198

572 **15.** Kebede, A. F., Nieborak, A., Shahidian, L. Z., Le Gras, S., Richter, F., Gómez, D. A. et al Histone
573 propionylation is a mark of active chromatin. Nat Struct Mol Biol 2017;**24**:1048-1056
574 **16.** Farrelly, L. A., Thompson, R. E., Zhao, S., Lepack, A. E., Lyu, Y., Bhanu, N. V. et al Histone
575 serotonylation is a permissive modification that enhances TFIID binding to H3K4me3. Nature
576 2019;**567**:535-539
577 **17.** Zhang, D., Tang, Z., Huang, H., Zhou, G., Cui, C., Weng, Y. et al. Metabolic regulation of gene
578 expression by histone lactylation. Nature **574**,575-580 (2019)
579 **18.** Lepack, A.E., Werner, C.T., Stewart, A.F., Fulton, S.L., Zhong, P., Farrelly, L.A. et al.
580 Dopaminylation of histone H3 in ventral tegmental area regulates cocaine seeking. Science **368**,
581 197-201 (2020)
582 **19.** Mews, P., Donahue, G., Drake, A.M., Luczak, V., Abel, T., Berger, S.L. Acetyl-CoA synthetase
583 regulates histone acetylation and hippocampal memory. Nature 2017; 546, 381–386
584 **20.** Wellen, K.E., Hatzivassiliou, G., Sachdeva, U.M., Bui, T.V., Cross, J.R., Thompson, C.B. ATP-
585 citrate lyase links cellular metabolism to histone acetylation. Science2009; 324, 1076–1080
586 **21.** Mews, P., Egervari, G., Nativio, R., Sidoli, S., Donahue, G., Lombroso, S.I. Alcohol metabolism
587 contributes to brain histone acetylation. Nature 2019; 574, 717–721
588 **22.** Tanaka, T., Yoshida, N., Kishimoto, T., Akira, S. Defective adipocyte differentiation in mice
589 lacking the C/EBPbeta and/or C/EBPdelta gene. EMBO J. 1997; 16, 7432–7443.
590 **23.** Hamm, J.K., Park, B.H., Farmer, S.R. A role for C/EBPbeta in regulating peroxisome proliferator-
591 activated receptor gamma activity during adipogenesis in 3T3-L1 preadipocytes. J. Biol. Chem.
592 2001; 276, 18464–18471.
593 **24.** Gao, M. et al. Metabolically controlled histone H4K5 acylation/acetylation ratio drives BRD4
594 genomic distribution. Cell Rep 2021; 36(4):109460.

595 **25.** Xiao, Y. et al. HBO1 is a versatile histone acyltransferase critical for promoter histone acylations.
596 Nucleic Acids Res 2021; 49(14):8037-8059.

597 **26.** Carrer, A., Parris, J. L., Trefely, S., Henry, R. A., Montgomery, D. C., Torres, A. et al Impact of a
598 High-fat Diet on Tissue Acyl-CoA and Histone Acetylation Levels. J Biol Chem 2017;**292**:3312-
599 3322

600 **27.** Burgeois, C., Gorwood, J., Barrail-Tran, A., Lagathu, C., Capeau, J., Desjardins, D. et al. Specific
601 Biological Features of Adipose Tissue, and their impact on HIV persistence. Front Microbiol **17**
602 (2019)

603 **28.** Trapnell, C., Roberts, A., Goff, L., Pertea, G., Kim, D., Kelley et al Differential gene and transcript
604 expression analysis of RNA-seq experiments with TopHat and Cufflinks. Nat Protoc 2012;**7**:562-
605 578

606 **29.** Thomas, P. D., Campbell, M. J., Kejariwal, A., Mi, H., Karlak, B., Daverman, R. et al PANTHER: a
607 library of protein families and subfamilies indexed by function. Genome Res 2003;**13**:2129-2141

608 **30.** de Hoon, M. J. L., Imoto, S., Nolan, J.,Miyano, S. Open source clustering software. Bioinformatics
609 2004;**9**:1453-1454

610

611

612

613

614

615

616

Figure 1

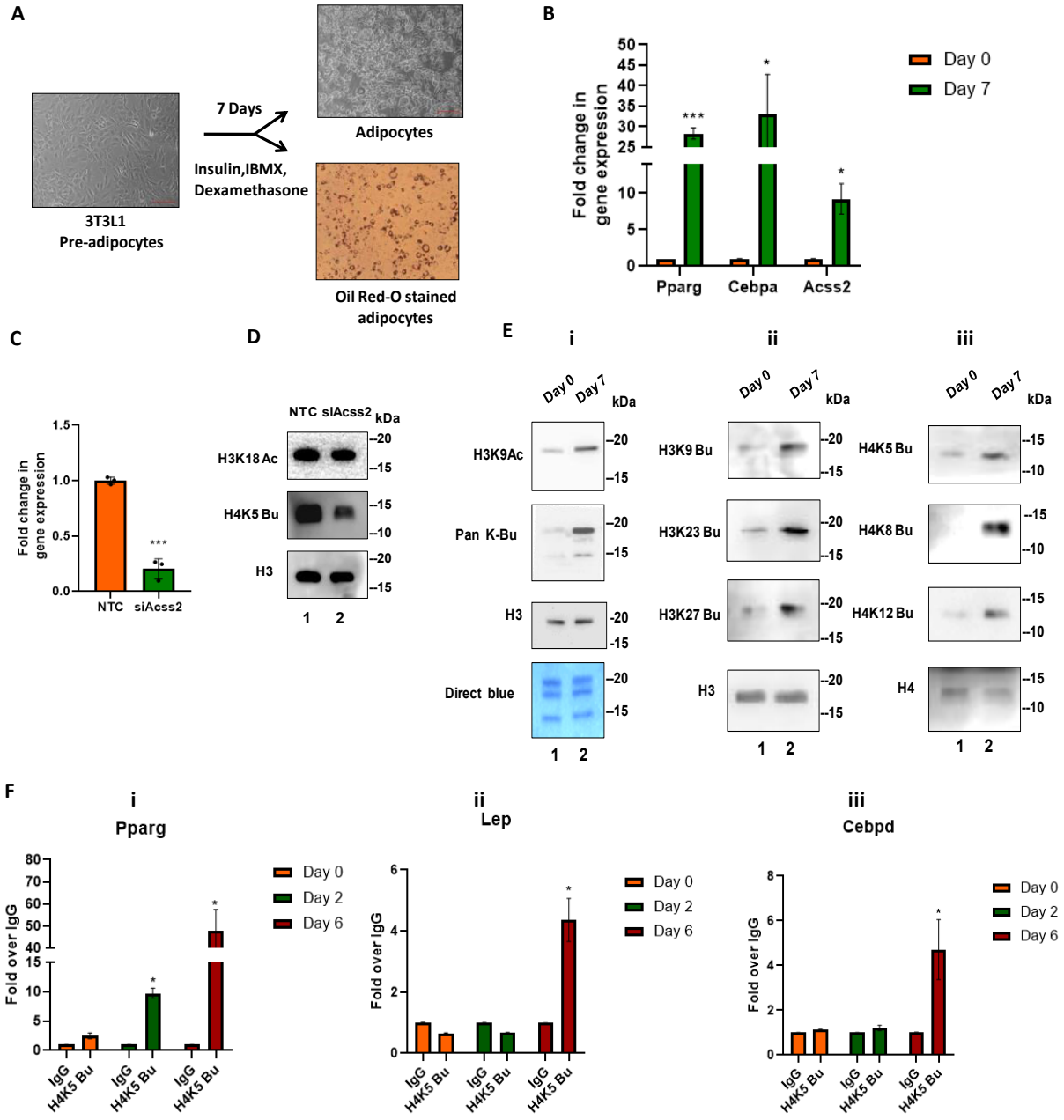

617

618

619

620

621

622

623 **Fig.1 Histone butyrylation increases during adipogenesis** (A) Phase contrast images of 3T3L1 cells
624 exhibiting fibroblast like morphology in their pre-adipocyte state and accumulation of lipid droplets in
625 their adipocyte state. The lipid droplets can be stained using Oil Red-O dye. (B) RT-qPCR analysis was
626 performed to check for transcript levels of Acss2 in undifferentiated and differentiated 3T3L1 cells. Error
627 bars denote mean +/- SEM of three biological replicates; two-tailed unpaired Student's t-test: * $P < 0.05$,
628 **$P < 0.01$, ***$P < 0.001$, ns: not significant. (C) Knockdown of Acss2 in differentiated 3T3L1 cells was
629 confirmed by RT-qPCR analysis. Error bars denote mean +/- SEM of three biological replicates; two-tailed
630 unpaired Student's t-test: * $P < 0.05$, **$P < 0.01$, ***$P < 0.001$, ns: not significant. (D) Histone
631 acetylation and butyrylation pattern in 3T3L1 cells upon Acss2 knockdown was checked using antibodies
632 against acetylated histone H3K18 and butyrylated H4K5. (E) Histone acetylation and butyrylation levels
633 in 3T3L1 cells in undifferentiated and differentiated state were analysed by immunoblotting with
634 antibodies specific for acetylated H3K9, butyrylated H3K9, H3K23, H3K27, H4K5, H4K8, H4K12 and pan-
635 butyryl lysine antibodies . Antibodies against core histones H3 and H4 were used as loading controls
636 along with Direct Blue staining of all four core histones. Lane 1- undifferentiated pre-adipocyte (Day 0)
637 and Lane 2 - differentiated adipocyte (Day 7) in each of the panels i, ii and iii. (F) Enrichment of H4K5
638 butyrylation in the promoters of (i) Pparg, (ii) Lep and (iii) Cebpd represented in the form of fold change
639 over IgG. Error bars denote mean +/- SEM of three biological replicates; one-way ANOVA with Dunnett's
640 multiple comparision was performed: * $P < 0.05$, **$P < 0.01$, ***$P < 0.001$, ns: not significant.

641

642

643

644

645

646

647

648

649

650

651

652

653

654

Figure 2

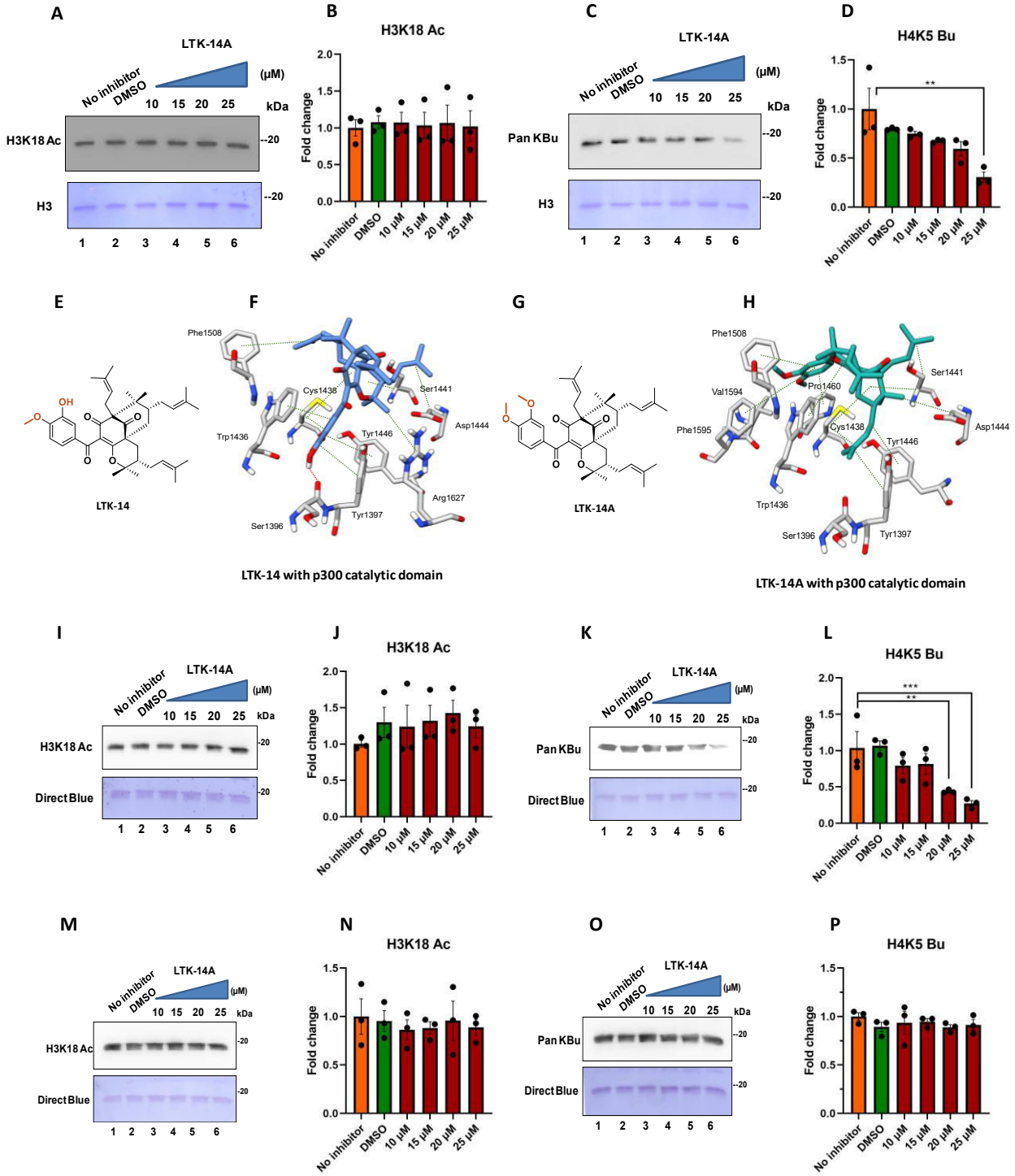

655

656

657

Figure 2: LTK-14A selectively inhibits p300 catalysed butyrylation without affecting its acetyltransferase activity: Immunoblotting with antibodies against acetylated H3K18 (A) and pan-butyryl lysine (C) to check for the relative inhibition of acetyltransferase and butyryltransferase activities of full length p300 by LTK-14A at different concentrations. Recombinant histone H3 was used as substrate. Lane 1, enzyme alone; Lane 2, enzyme + DMSO; Lane 3-6, enzyme + LTK-14A at concentrations 10, 15, 20 and 25 µM respectively. Images of Western blotting are given in panels F and H and their quantitations are given in panels B and D. Molecular structures of mono- (LTK-14) and di- (LTK-14A) substituted isogarcinol (E and G). Molecular docking studies for studying comparative interaction of LTK-14 and LTK-14A with the amino acid residues of p300 catalytic domain (F and H). The predicted interactions are denoted by tick lines. Hydrogen bonding is shown in red and hydrophobic interaction is shown in green. Immunoblotting with antibodies against acetylated H3K18 (I) and pan-butyryl lysine (K) to check for the relative inhibition of acetyltransferase and butyryltransferase activities of wild type p300 catalytic domain by LTK-14A at different concentrations. Lane 1, enzyme alone; Lane 2, enzyme + DMSO; Lane 3-6, enzyme + LTK-14A at concentrations 10, 15, 20 and 25 µM respectively. Images of Western blotting are given in panels I and K and their quantitations are given in panels J and L. Immunoblotting with antibodies against acetylated H3K18 (M) and pan-butyryl lysine (O) to check for the relative inhibition of acetyltransferase and butyryltransferase activities of catalytically active p300 catalytic domain with point mutation C1438A by LTK-14A at different concentrations. Lane 1, enzyme alone; Lane 2, enzyme + DMSO; Lane 3-6, enzyme + LTK-14A at concentrations 10, 15, 20 and 25 µM respectively. Images of Western blotting are given in panels M and O and their quantitation are given in panels N and P. Error bars denote mean +/- SEM of three biological replicates, one-way ANOVA with Bonferroni's multiple comparison; * $P < 0.05$, ** $P < 0.01$, *** $P < 0.001$, ns: not significant.

Figure 3

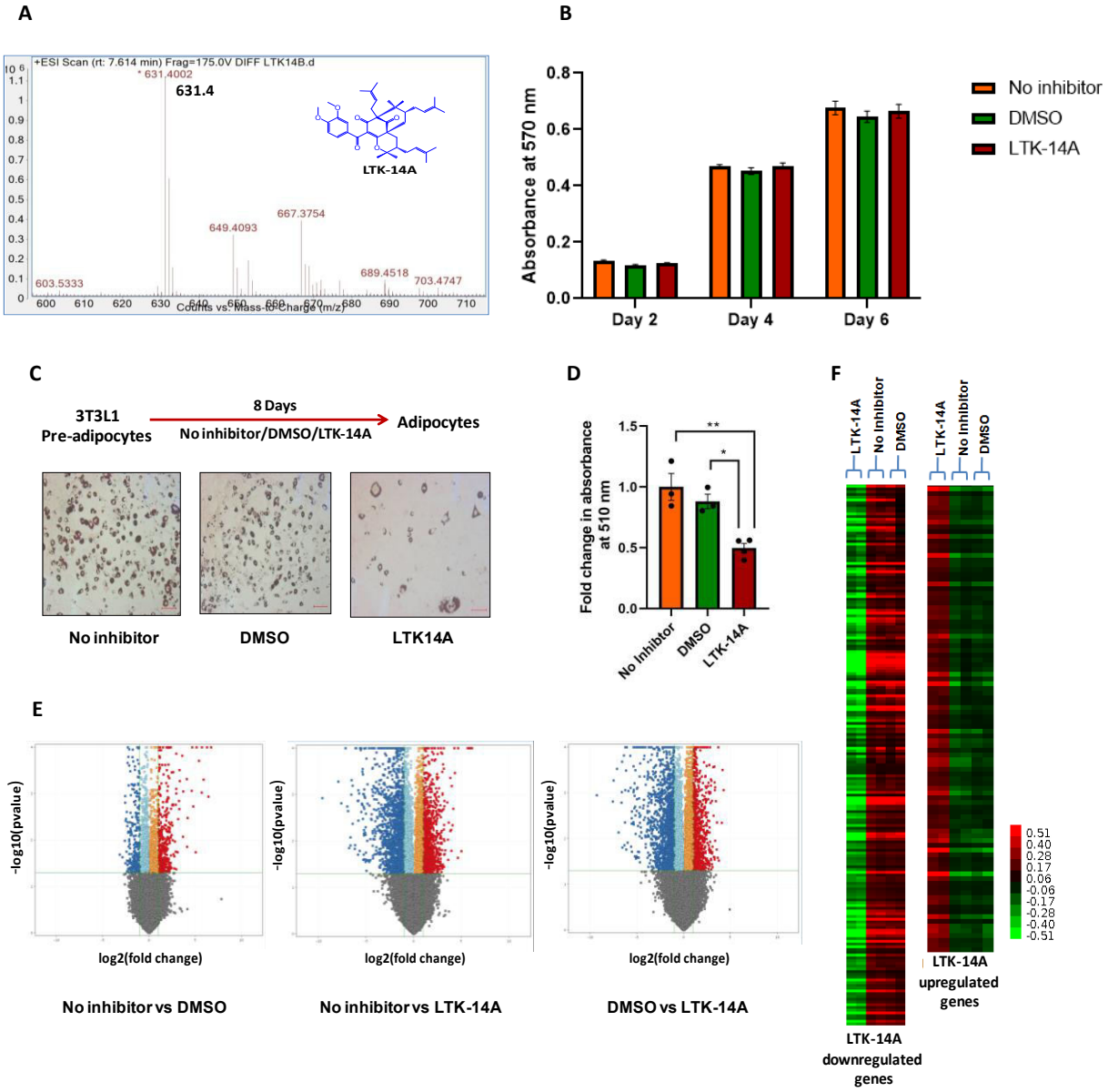
A
+ESI Scan (rt: 7.614 min) Frag=175.0V DIFF LTK14B.d
631.4
LTK-14A
667.3754
649.4093
603.5333
689.4518
703.4747
Counts vs. Mass-to-Charge (m/z)
B
Absorbance at 570 nm
Day 2
Day 4
Day 6
No inhibitor
DMSO
LTK-14A
C
3T3L1
Pre-adipocytes
8 Days
No inhibitor/DMSO/LTK-14A
Adipocytes
No inhibitor
DMSO
LTK14A
D
Fold change in absorbance at 510 nm
No Inhibitor
DMSO
LTK-14A
E
-log10(pvalue)
log2(fold change)
No inhibitor vs DMSO
No inhibitor vs LTK-14A
DMSO vs LTK-14A
F
LTK-14A
No Inhibitor
DMSO
LTK-14A upregulated genes
LTK-14A downregulated genes

699 **Fig. 3: The butyrylation inhibitor represses adipogenesis in 3T3L1 cells:** (A) The permeability and
700 stability of LTK-14A in 3T3L1 was tested by LC-ESI-MS analysis of metabolites, extracted from the
701 compound treated 3T3L1 cells to detect the protonated LTK-14A in the ESI spectra of the eluted fraction.
702 (B) MTT assay was performed to check for any possible cellular toxicity effect of LTK-14A, using 25 µM
703 concentration of the compound on 3T3L1 cells upon incubation for varying lengths of time (2, 4 and 6
704 days). Comparison was done with cells that were left untreated or treated with DMSO as solvent
705 control. The effect of LTK-1a4A (25 µM) treatment on adipogenesis was tested by Oil Red-O staining of
706 the adipocytes (C) and the quantitation of staining is represented graphically in panel D. Error bars
707 denote mean +/- SEM of three biological replicates,one-way ANOVA with Bonferroni's multiple
708 comparison; * $P < 0.05$, ** $P < 0.01$, *** $P < 0.001$, ns: not significant. (E) The effect of LTK-14A on the
709 global transcription network inside 3T3L1 cells was investigated by high throughput transcriptome
710 analysis with RNA isolated from compound treated, DMSO treated and untreated 3T3L1 cells (n=2 in
711 each case). Differential gene expression pattern of three conditions compared with each other, depicted
712 in volcano plots- No Inhibitor versus DMSO , No Inhibitor versus LTK-14A and DMSO versus LTK-14A. The
713 downregulated and upregulated genes are shown in blue and red respectively.(F) Heat maps showing
714 the differential gene expression pattern between LTK-14A treated cells and DMSO treated or untreated
715 cells.

716

717

718

719

720

721

722

723

724

725

726

727

728

729

730

Figure 4

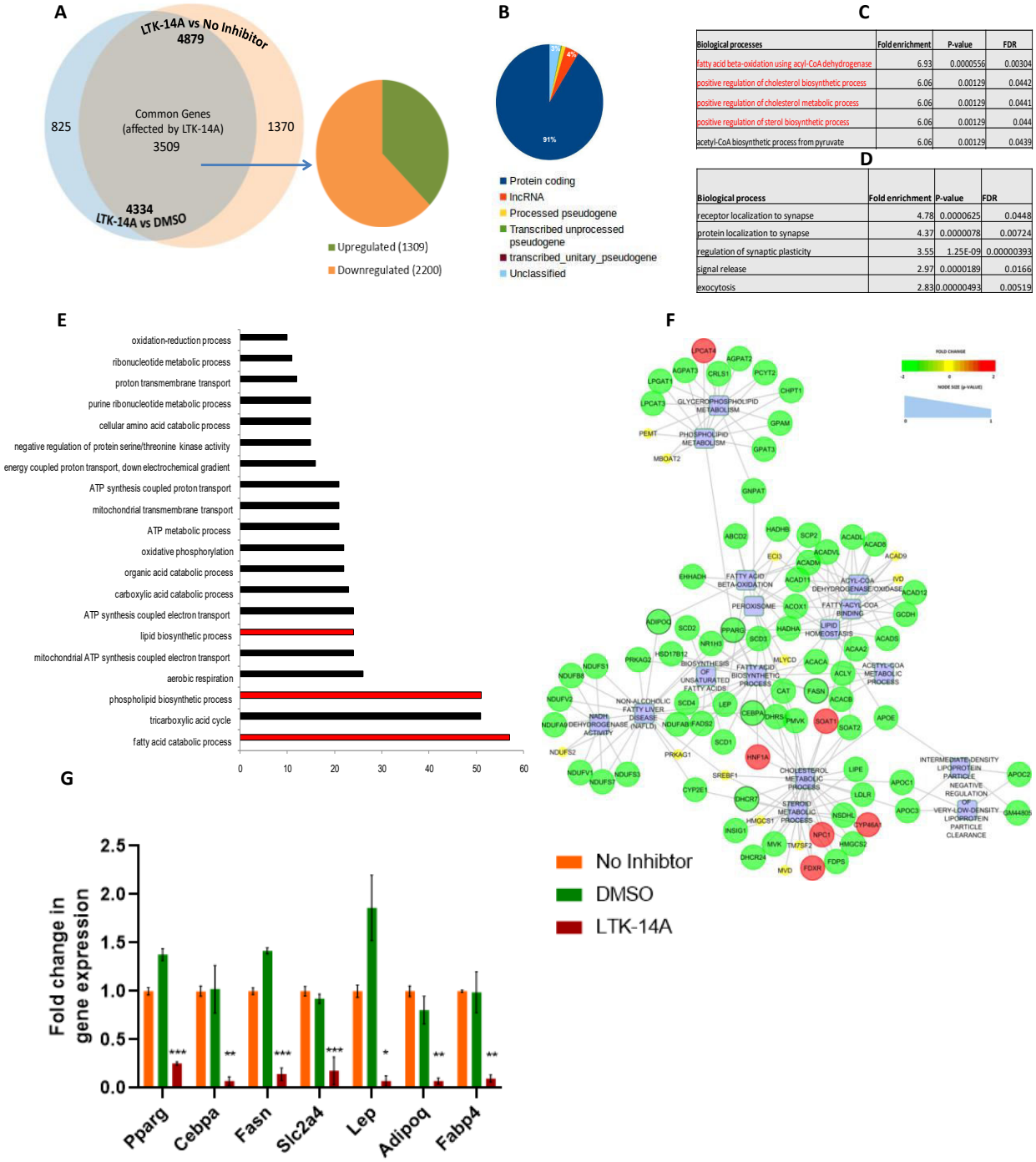

Biological processes	Fold enrichment	P-value	FDR
fatty acid beta-oxidation using acyl-CoA dehydrogenase	6.93	0.0000556	0.00304
positive regulation of cholesterol biosynthetic process	6.06	0.00129	0.0442
positive regulation of cholesterol metabolic process	6.06	0.00129	0.0441
positive regulation of sterol biosynthetic process	6.06	0.00129	0.044
acetyl-CoA biosynthetic process from pyruvate	6.06	0.00129	0.0439

Biological process	Fold enrichment	P-value	FDR
receptor localization to synapse	4.78	0.0000625	0.0448
protein localization to synapse	4.37	0.0000078	0.00724
regulation of synaptic plasticity	3.55	1.25E-09	0.00000393
signal release	2.97	0.0000189	0.0166
exocytosis	2.83	0.00000493	0.00519

735 **Figure 4: LTK-14A represses expression of several pro-adipogenic genes and inhibits lipid metabolism:**
736 (A) Venn diagram showing the number of differentially expressed genes upon LTK-14A treatment with
737 respect to untreated and DMSO treated conditions. (B) Classification of the common differentially
738 expressed genes according to their type. Gene ontology analysis was performed to study the different
739 biological pathways that were affected by LTK-14A in 3T3L1 compared to DMSO treated as well as
740 untreated conditions, as predicted by Panther software. The pathways were ranked in the order of
741 those with maximum number of genes affected (E). A different ranking order was created on the basis of
742 fold enrichment i.e. the pathways in which the ratio of number of observed affected genes over number
743 of expected genes to be affected was the highest (C). A similar analysis was also performed for genes
744 differentially expressed in DMSO versus untreated conditions (D). (F) A molecular network was
745 constructed to depict the interconnectivity between the lipid metabolism related genes and pathways
746 that were affected upon their dysregulation by LTK-14A compared to DMSO treated conditions. (G) RT-
747 qPCR analysis was performed to validate the putative target genes of LTK-14A. Error bars denote mean
748 +/- SEM of three biological replicates; one-way ANOVA with Bonferroni's multiple comparison: * $P < 0.05$, ** $P < 0.01$, *** $P < 0.001$, ns: not significant.

750

751

752

753

754

755

756

757

758

759

760

761

762

763

764

765

Figure 5

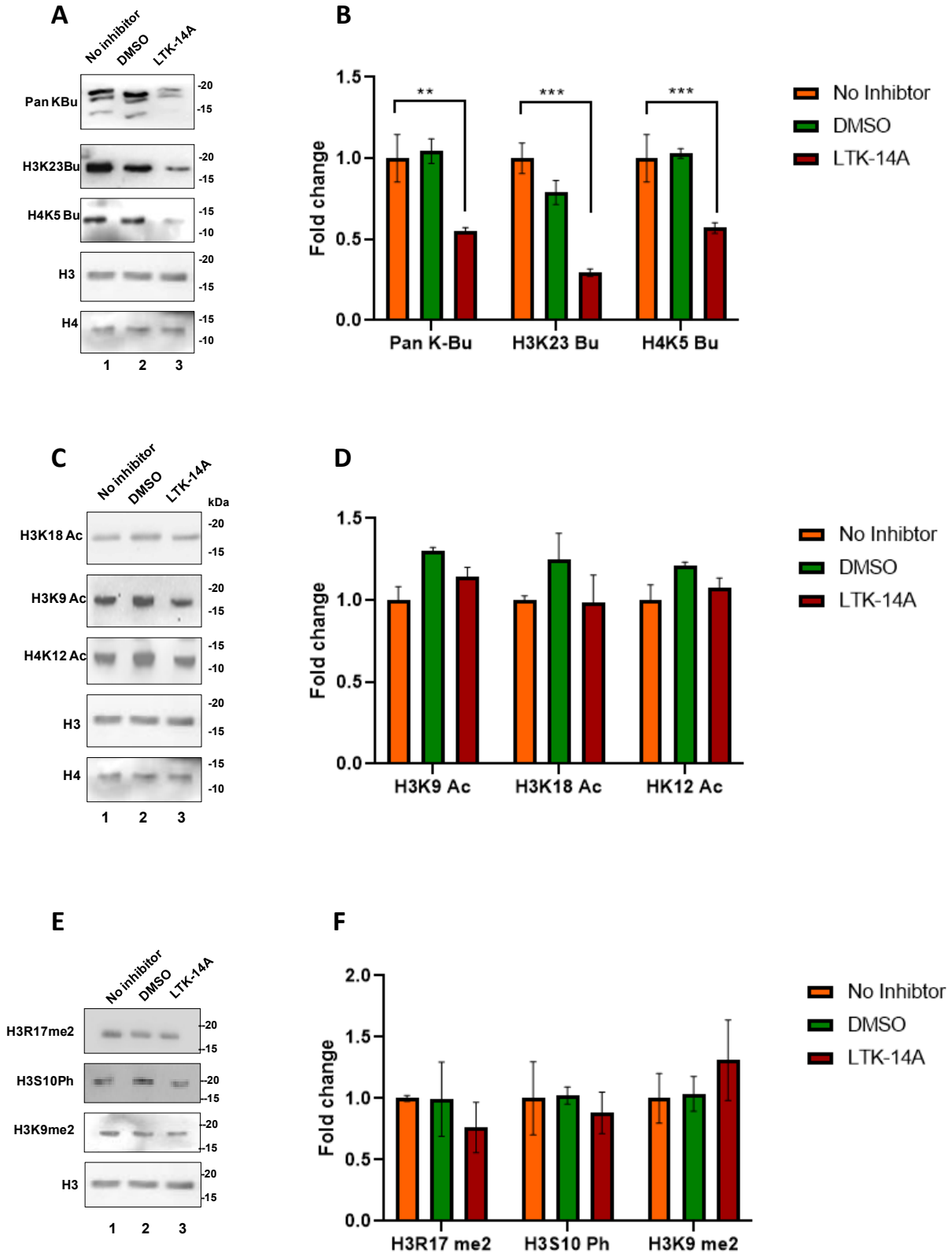
A
No inhibitor
DMSO
LTK-14A
Pan KBu
H3K23Bu
H4K5 Bu
H3
H4
-20
-15
-10
1
2
3
B
Fold change
1.5
1.0
0.5
0.0
**
***
***
Pan K-Bu
H3K23 Bu
H4K5 Bu
No Inhibtor
DMSO
LTK-14A
C
No inhibitor
DMSO
LTK-14A
kDa
H3K18 Ac
H3K9 Ac
H4K12 Ac
H3
H4
-20
-15
-10
1
2
3
D
Fold change
1.5
1.0
0.5
0.0
H3K9 Ac
H3K18 Ac
HK12 Ac
No Inhibtor
DMSO
LTK-14A
E
No inhibitor
DMSO
LTK-14A
H3R17me2
H3S10Ph
H3K9me2
H3
-20
-15
1
2
3
F
Fold change
2.0
1.5
1.0
0.5
0.0
H3R17 me2
H3S10 Ph
H3K9 me2
No Inhibtor
DMSO
LTK-14A

766

767 **Fig.5: LTK-14A inhibits histone butyrylation in 3T3L1 cells, without affecting acetylation or other post-**
768 **translational modifications**: Histone butyrylation levels in 3T3L1 cells that were treated with LTK-14A
769 were compared with that in DMSO treated and untreated conditions by immunoblotting with antibodies
770 against butyrylated histone H3K23 , H4K5 and pan-butyryl lysine. Histones H3 and H4 were used as
771 loading controls (A). The fold change of quantified band intensity is graphically represented in panel (B)
772 in which the error bars denote mean +/- SEM of three biological replicates. Under similar conditions
773 histone acetylation levels were compared by immunoblotting using antibodies against acetylated
774 histones H3K18, H3K9 and H4K12 (C). The result is graphically represented in panel (D) in which error
775 bars denote mean +/- SEM of three biological replicates. Immunoblotting was also performed with
776 antibodies against histone H3R17 dimethylation, H3S10 Phosphorylation and H3K9 dimethylation (E).
777 The result is graphically represented in panel F in which error bars denote mean +/- SEM of three
778 biological replicates. For all data one-way ANOVA with Bonferroni's multiple comparision was
779 performed: * $P < 0.05$, ** $P < 0.01$, *** $P < 0.001$, ns: not significant .

780

781

782

783

784

785

786

787

788

789

790

791

792

793

794

795

796

Figure 6

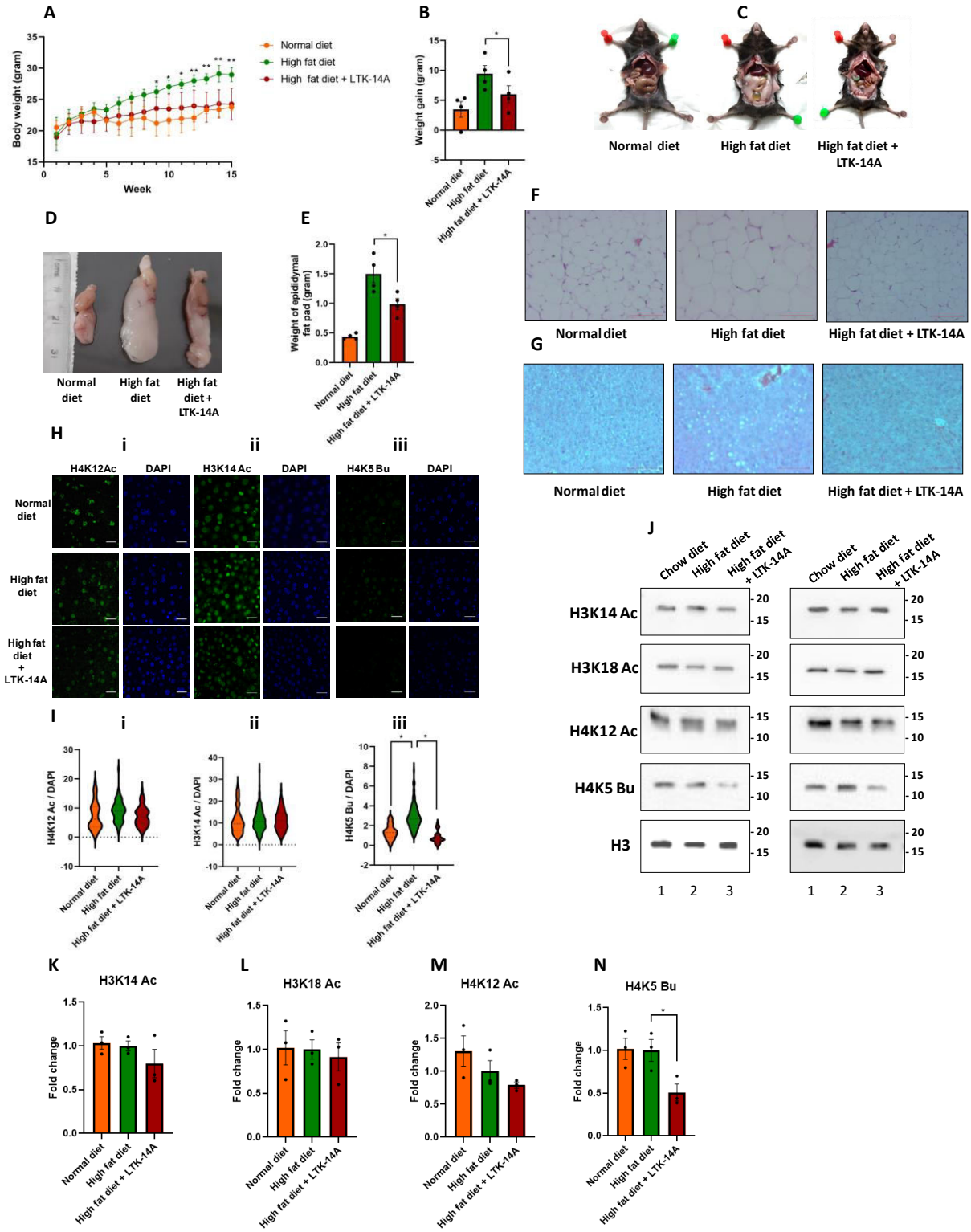

797

798

799

800 **Fig. 6: The weight gaining of high fat diet fed mice (C57BL6/J) could be significantly reduced by the**
801 **butyrylation specific inhibitor of p300:** Trend of weight gaining (A) and average body weight gained
802 after 16 weeks (B) of C57BL6/J mice maintained on normal chow diet, high fat diet and high fat diet
803 mixed with LTK-14A was plotted; n=4 in each group. Representative images of dissected bodies showing
804 fat accumulation (C) and epididymal fat pads (D) of the mice from three groups. The average weight of
805 the fat pads is represented graphically (E); n=4 in each group. Representative images of morphology of
806 adipose tissue (F) and liver (G) from the mice of the three groups, as studied by hematoxylin and eosin
807 staining. For all data one-way ANOVA with Dunnett's multiple comparision was performed: * $P < 0.05$,
808 ** $P < 0.01$, *** $P < 0.001$, ns: not significant. (H) Immunofluorescence microscopy of liver sections
809 stained with antibodies against histone H4K12 acetylation (panel i), histone H3K14 acetylation (panel ii)
810 and histone H4K5 butyrylation (panel iii). The fluorescence intensity of the modified histone marks was
811 normalised against DAPI staining of whole nuclei for quantitation which is graphically depicted in (I)
812 panel i, ii and iii ;n=4 in each group; one-way ANOVA with Dunnett's multiple comparision: * $P < 0.05$,
813 ** $P < 0.01$, *** $P < 0.001$, ns: not significant. (J) Histone H3K14, H3K18, H4K12 acetylation and H4K5
814 butyrylation levels in epididymal fat pads of mice were estimated by immunoblotting . Histone H3 was
815 used as loading control The fold change of quantified band intensity is graphically represented in panel
816 K,L, M and N ;n=3 in each group; one-way ANOVA with Dunnett's multiple comparision: * $P < 0.05$, ** $P <$
817 0.01, *** $P < 0.001$, ns: not significant.

818

819

820

821

822

823

824

825

826

827

828

829

830

831

Figure 7

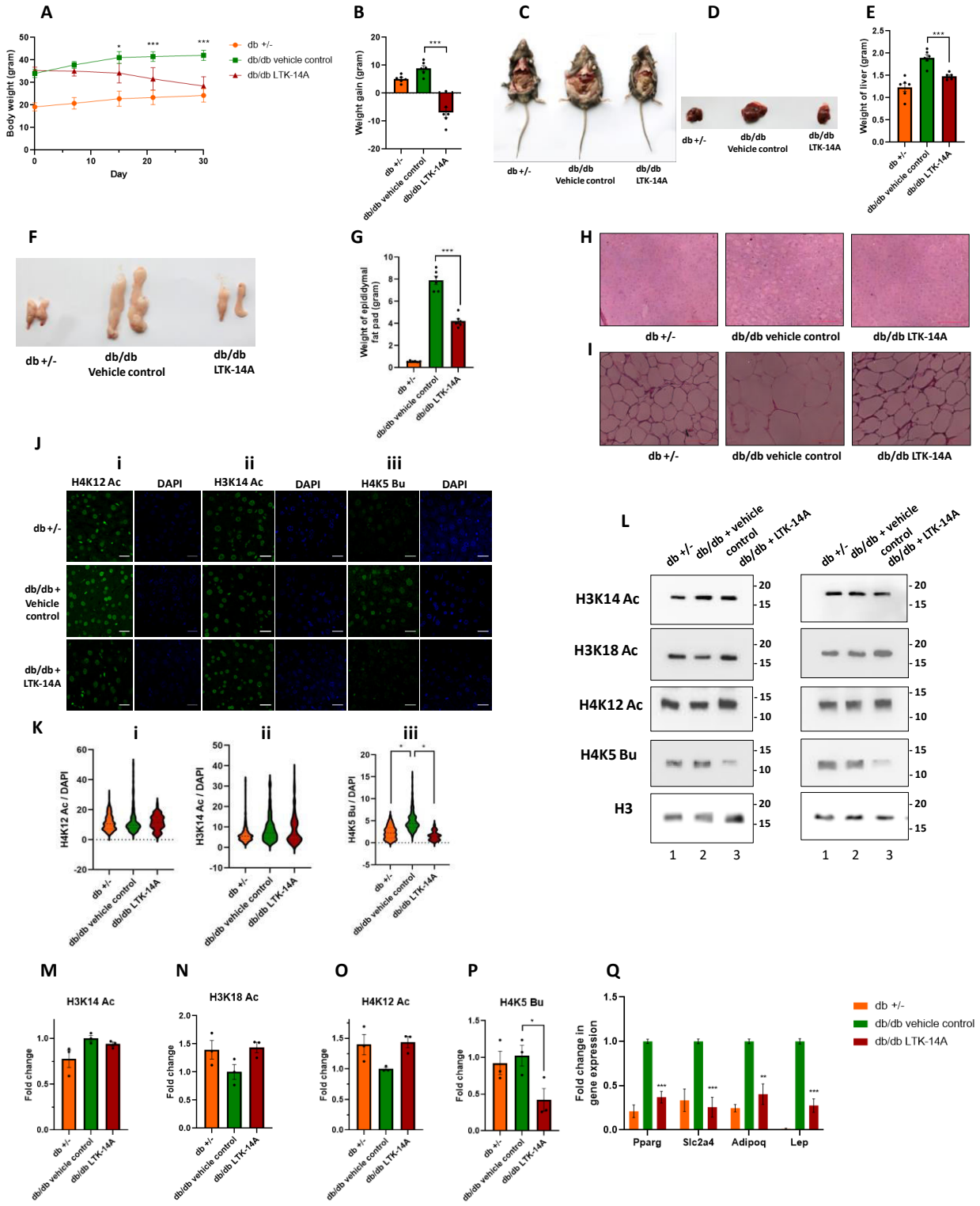

832

833

834

835 **Fig. 7: Oral gavaging of the butyrylation inhibitor reduces weight of genetically obese db/db mice:**
836 Trend of weight gaining (A) and average body weight gained after 30 days (B) of db +/- and db/db mice
837 orally administered with either LTK-14A or vehicle solution ; n=6 in each group. (C) Representative
838 images of dissected bodies showing fat accumulation (panel iii) of the mice from three groups.
839 Representative images of liver (D) from the mice of three groups and average weight of liver (E)
840 depicted graphically; n= 6 in each group. Representative images of epididymal fat pads (F) from the mice
841 of three groups and average weight of fat pads (G) depicted graphically; n= 6 in each group.
842 Representative images of morphology of liver (H) and adipose tissue (I) from the mice of the three
843 groups, as studied by hematoxylin and eosin staining. (J) Immunofluorescence microscopy of liver
844 sections stained with antibodies against histone H4K12 acetylation (panel i), histone H3K14 acetylation
845 (panel ii) and histone H4K5 butyrylation (panel iii). The fluorescence intensity of the modified histone
846 marks was normalised against DAPI staining of whole nuclei for quantitation which is graphically
847 depicted in (K) panel i, ii and iii ;n=4 in each group; one-way ANOVA with Dunnett's multiple
848 comparision: * $P < 0.05$, ** $P < 0.01$, *** $P < 0.001$, ns: not significant. (L) Histone H3K14, H3K18, H4K12
849 acetylation and H4K5 butyrylation levels in epididymal fat pads of mice were estimated by
850 immunoblotting. Histone H3 was used as loading control The fold change of quantified band intensity is
851 graphically represented in panel M,N, O and P; n=3 in each group; one-way ANOVA with Dunnett's
852 multiple comparision: * $P < 0.05$, ** $P < 0.01$, *** $P < 0.001$, ns: not significant. (Q) qRT-PCR with RNA
853 isolated from epididymal fat pads to check the expression pattern of lipogenesis related pro-adipogenic
854 genes upon LTK-14A treatment; n=3/4 in each group; one-way ANOVA with Dunnett's multiple
855 comparision: * $P < 0.05$, ** $P < 0.01$, *** $P < 0.001$, ns: not significant

856

857

858

859

860

861

862

863

864

865

866

867

Graphical abstract

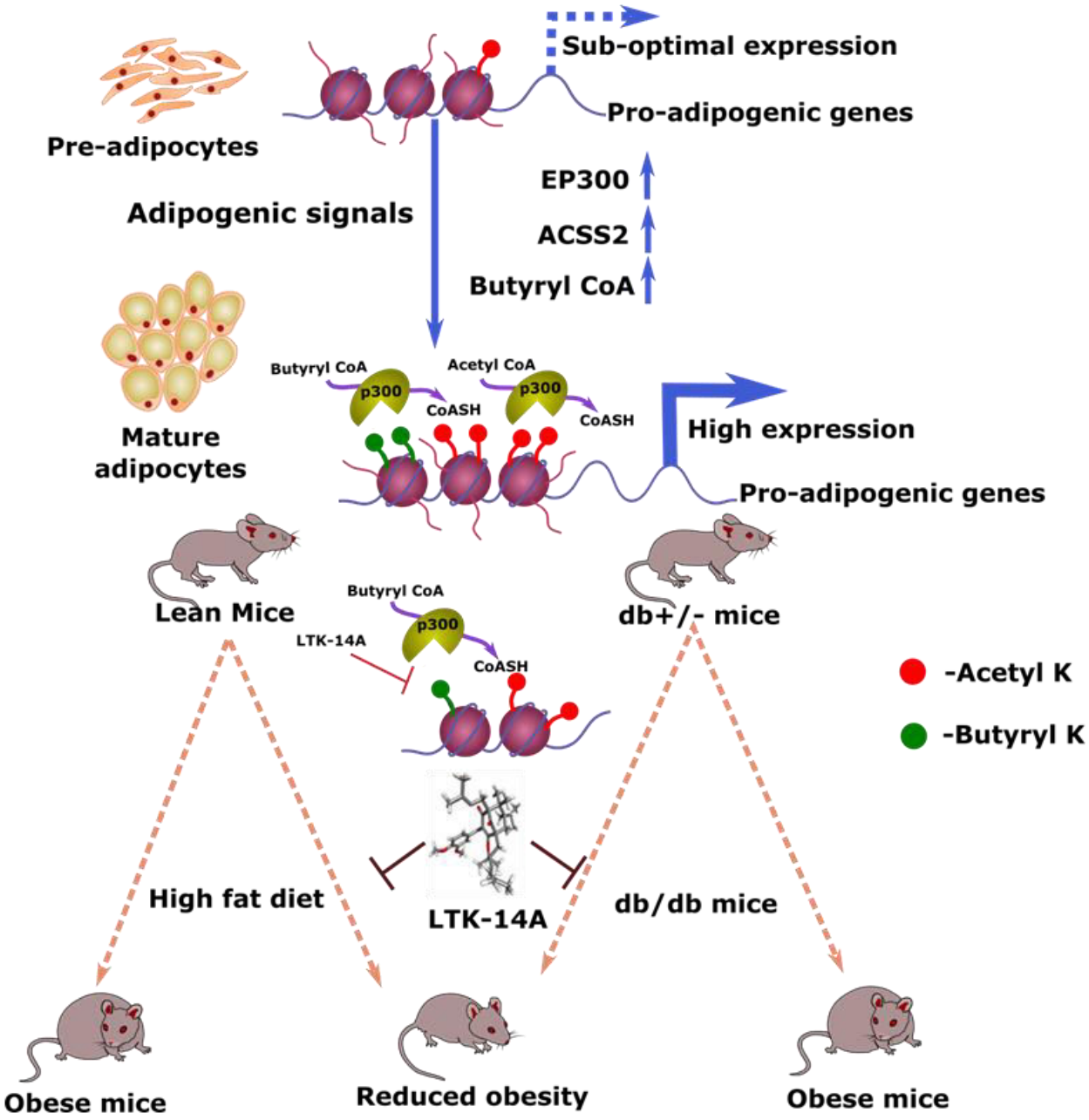

872 **Graphical abstract:**

873 **Proposed model for the role of p300-mediated histone butyrylation in adipogenesis:**

874 In pre-adipocytes, there exists a basal level of histone acetylation while butyrylation is present to a
875 much lesser extent owing to low stoichiometric levels of butyryl CoA. Induction of adipogenesis causes a
876 simultaneous upregulation of histone acetylation and butyrylation marks leading to increased rate of
877 adipogenesis and concomitant transcriptional activation of pro-adipogeneic genes.

878 Onset of obesity in mice, either due to excess energy intake through high fat diet consumption or
879 increased de novo synthesis of fatty acids due to leptin receptor gene mutation leading to hyperphagic
880 behavior, is accompanied by adipocyte hyperplasia and hypertrophy. Both the organs of adipose tissue
881 and liver were found to have enhanced levels of H4K5 butyrylation during obesity. LTK-14A, a
882 butyrylation specific inhibitor could efficiently prevent the processes of adipogenesis and adipocyte
883 hypertrophy due to inhibition of H4K5 butyrylation in these organs. Thus the compound could attenuate
884 weight gain by selective inhibition of butyrylation without affecting acetylation, thereby highlighting the
885 importance of histone butyrylation in adipogenesis and obesity.

886

887

888

889

890

891

892

893

894

895

896

897

898

899

900

901 **Supplementary Section:**

902 **Supplementary Materials and Methods:**

903 **siRNA experiments:** ON-TARGETplus siRNA SMART pools against mouse Acss2 (catalog no.L-065412-01-
904 0005) was purchased from Dharmacon (Dharmacon, Lafayette, CO, USA). 3T3L1 cells were transfected
905 with Acss2 siRNA at 25 nM concentration, using RNAiMAX (catalog no. 13778-150, Thermo Fisher
906 Scientific) according to manufacturer's protocols. Transfection was carried out for 48 hours after which
907 cells were induced for differentiation for 6 days followed by RNA isolation and histone extraction.

908 **Molecular docking analysis:** Glide module of Schrodinger suite was used to dock LTK-14 and LTK-14A to
909 p300 catalytic domain (PDB: 3BIY). Chimera was used as visualizing software. The protein was prepared
910 using the wizard tool in Maestro version 10.2.The crystal structure of LTK-14A (CCDC 1969185) and LTK-
911 14 (CCDC 645420) were used as the most optimized and energy minimized ligand structures. The
912 receptor grid for p300 catalytic domain was generated by specifying the binding (active) site residues
913 using Receptor grid generation in the Schrodinger Glide application. Once the receptor grid was
914 generated, the ligands LTK-14 and LTK-14A were docked to the p300 catalytic domain using Glide
915 version 5.8 molecular docking.

916 **Untargeted analysis of intracellular metabolites by Ultra-performance liquid chromatography coupled**
917 **with time-of-flight mass spectrometer (Q-TOF LC/MS):** Profiling of intracellular metabolites was
918 performed on an agilent 1290 Infinity LC system coupled to Agilent 6545 Accurate-Mass Quadrupole
919 Time-of- Flight (QTOF) with Agilent Jet Stream Thermal Gradient Technology. The UPLC system was
920 assembled with a Diode array detector (DAD) and autosampler. The Chromatographic separation was
921 achieved on Agilent ZORBAX SB- C18 column (2.1 × 100 mm, 1.8 µm) as stationary phase. The mobile
922 phase consisted of a linear gradient of 100 mM ammonium formate (A) and Acetonitrile (B): 0–10.0 min,
923 30-80% B (v/v); 10.0–15.0 min, 80–100% B (v/v); 15.0–20.0 min, 100% B (v/v); 20.0–21.0 min, 100–30%
924 B (v/v); 21.0–25.0 min, 30% B. The sample was dissolved in 1 ml methanol (LCMS Grade), centrifuged
925 and supernatant was taken for UPLC-QTOF-MS analysis. The column was reconditioned for 5 minutes
926 prior to the next injection. The flow rate was 0.5 ml/min, and the injected volume was 20 µL. The UPLC
927 was connected to the MS analysis was performed on an Agilent 6545 Accurate-Mass Q-TOF/MS system
928 with an electrospray ionization (ESI) source. Considering the MS conditions, positive ion mode was used
929 to obtain high-resolution mass spectra. The ESI source parameters were: drying gas (N2) flow, 8 L/min;
930 drying gas temperature, 200°C. Other parameters were set as nebuliser gas, 35 psig; capillary voltage,
931 3000 V; skimmer voltage, 65 V; nozzle voltage 1000 V and fragmentor voltage 150 V. The data
932 acquisition on the LC-QTOF was performed using Agilent Mass Hunter Acquisition software (Agilent
933 Technologies, Santa Clara, CA, USA). The data were deconvoluted into individual chemical peaks with
934 Agilent MassHunter Qualitative Analysis (MassHunterQual, Agilent Technologies).

935 **Site directed mutagenesis:** Point mutation was introduced into the p300 catalytic domain sequence
936 cloned within pET-28b plasmid by using the Quikchange site directed mutagenesis kit (Agilent). Briefly,
937 the template was mixed with Pfuturbo DNA polymerase, designed forward and reverse primers and
938 dNTPs for PCR (Initial denaturation for 30 seconds at 95°C; Cycles: 95°C 30'', 55°C for 60'', 68°C for 7';

939 final elongation at 68°C for 5'.) The mixture was then incubated with DpnI enzyme for 2.5 hours for
940 removal of the parent wild type sequence followed by transformation of competent XL10Gold cells and
941 kanamycin selection of positive transformants. The inserted mutation was verified by sequencing and
942 alignment with the wild type sequence using ClustalOmega software. The sequences of the primers used
943 are as follows:

944 Forward primer- 5'- CCTCACTTGGTGGAGCTGCCCAAAATATGCCCTGTTGTG – 3'

945 Reverse primer- 5'- CACAACAGGGCATATTTGGGCAGCTCCACCAAGTGAGG -3'

946

947 **Purification of recombinant full-length p300 and p300 catalytic domain:** Polyhistidine tagged
948 recombinant p300 was purified from Sf21 insect cells by Ni-NTA based affinity chromatography. These
949 cells were infected by the baculovirus containing p300 for 72 hours. Once the cells showed signs of
950 infection, they were scraped off and centrifuged to separate the spent media. The cell pellets were
951 resuspended in ice cold homogenisation buffer (20 mM Tris, pH 7.5; 20 mM imidazole, 10% glycerol, 0.2
952 mM EDTA, 300 mM KCl, 0.1%NP-40, 2 mM PMSF, 2 mM βmercaptoethanol) and then homogenised
953 using a Dounce homogeniser (5 cycles, 6 strokes per cycle with 5 minutes interval between each cycle).
954 The cell debris was separated by centrifugation and then the lysate was incubated with pre-equilibriated
955 Ni-NTA slurry for 2.5 hours at 4°C on an end-to-end rotor. Then the beads were washed with wash
956 buffer (20 mM Tris, pH 7.5; 40 mM imidazole) nine times to remove unwanted contaminants. Finally
957 p300 was eluted using elution buffer (20 mM Tris, pH 7.5; 250 mM imidazole).

958 Polyhistidine tagged p300 catalytic domain cloned in pET28b plasmid and Sirt2 were used for co-
959 transforming BL21(DE3) cells. At first, 50 ml primary culture was prepared in Luria broth containing
960 kanamycin (50 µg/ml) and ampicillin (100 µg/ml) (HIMEDIA) and then it was scaled up 10 times to
961 prepare secondary culture. Incubation was done at 37°C, 180 rpm till O.D. reached 0.37 followed by
962 induction with 0.2 mM IPTG and a further incubation at 30°C for 4 hours. Cells were pelleted at 6000
963 rpm, 4°C for 10 minutes and stored at -80°C. Resuspension and homogenisation of the pellet was
964 carried out in homogenisation buffer (20 mM Tris, pH 7.5; 20 mM imidazole, 10% glycerol, 0.2 mM
965 EDTA, 300 mM KCl, 0.1%NP-40, 2 mM PMSF, 2 mM βmercaptoethanol). 3 cycles of sonication were done
966 for 3 minutes at 35% amplitude with 5 minutes interval between each cycle. The cell debris were
967 separated by pelleting at 12000 rpm for 30 minutes at 4°C. The supernatant was equilibriated with Ni-
968 NTA beads slurry (Novagen) in an end-to-end rotor for 3 hours at 4 C. Eight washes were given with
969 wash buffer (20 mM Tris, pH 7.5; 40 mM imidazole). Elution was carried out in batches with elution
970 buffer (20 mM Tris, pH 7.5; 250 mM imidazole).

971 The enzymatic activity of the proteins was estimated by filter binding assay.

972

973 ***In vitro* filter binding assay:** Different dilutions of purified enzyme were incubated in reaction buffer (50
974 mM Tris-HCl pH 7.5, 1 mM DTT, 10 % Glycerol, 2 mM PMSF) with 10 mM NaBu, tritiated acetyl CoA (50

975 µCi) (PerkinElmer, Part No: NET290050UC) and Xenopus histone H3 (500 ng) for 30 minutes at 30°C. The
976 reaction mixture was then spotted on P81 filter paper and the paper was allowed to dry at room
977 temperature. The paper was washed in wash buffer (50 mM sodium bicarbonate and 50 mM sodium
978 carbonate), dried at 90°C and immersed in enhancing solution (2.5% PPO and 0.25% POPOP in toluene)
979 for taking radioactive counts using liquid scintillation counter (Perkin Elmer, MicroBeta2 system).

980

981 ***In vitro* acylation (acetylation/butyrylation) assay:** Acylation reactions were performed in reaction
982 buffer (25 mM Tris-HCl pH 7.5, 100 mM NaCl, 0.1 mM EDTA, 1 mM DTT, 10 % Glycerol, 1x PIC) with 100
983 ng/mL TSA, and 50 µM Butyryl-CoA/Acetyl CoA. Xenopus histone H3 (1 µg) was used as the substrate
984 and full length p300 or p300 catalytic domain (10,000 cpm activity) was used as the enzyme. Reactions
985 were incubated in presence or absence of butyrylation inhibitor for 10 minutes at 30 °C, followed by
986 initiation of the acetylation/butyrylation reaction by the addition of acetyl CoA/butyryl CoA. After a
987 further 10 minutes, reactions were stopped by addition of Laemmli buffer and samples were used for
988 immunoblotting.

989 **Transcriptomics analysis by RNA-seq:** RNA integrity was checked by Agilent Bioanalyzer 2100, only
990 samples with clean rRNA peaks were used. Libraries for RNA-seq were prepared according to KAPA
991 Stranded RNA-Seq Kit with RiboErase (KAPA Biosystems, Wilmington, MA) system. Final library quality
992 and quantity were analyzed by Agilent Bioanalyzer 2100 and Life Technologies Qubit3.0 Fluorometer,
993 respectively. 150 bp Paired-end sequencing was performed on Illumina HiSeq 4000 (Illumnia Inc., San
994 Diego, CA).

995 House mouse (Mus musculus, strain C57BL/6J) genome (mm10) was downloaded from GENCODE and
996 indexed using Bowtie2-build with default parameters. Adapter removal was done using Trim Galore (v
997 0.4.4) and each of the raw Fastq files were passed through a quality check using FastQC. PCR duplicates
998 were removed using the Samtools 1.3.1 with the help of 'rmdup' option. Each of the raw files was then
999 aligned to mm10 genome assembly using TopHat2 with default parameters for paired-end sequencing
1000 as described in (28). After aligning, quantification of transcripts was performed using Cufflinks and then
1001 Cuffmerge was used to create merged transcriptome annotation. Finally differentially expressed (DE)
1002 genes were identified using Cuffdiff. The threshold for DE genes was log2 (fold change) >1.5 for up
1003 regulated genes and log2 (fold change) <1.5 for down regulated genes with p-value <0.05.

1004 GO enrichment analysis

1005 Gene Ontology (GO) analysis was performed in PANTHER (29). Significant enrichment test was
1006 performed with the set of differentially expressed genes in PANTHER and Bonferroni correction method
1007 was applied to get the best result of significantly enriched biological processes.

1008 Fisher's exact test

1009 Fisher's exact test was performed in PANTHER Gene Ontology (GO) where p-value significance was
1010 calculated based on the ratio of obtained number of genes to the expected number of genes (O/E)
1011 considering the total number of genes for the respective pathway in Mus musculus with a FDR of <0.05.

1012 Heatmap and clustering of genes

1013 Unsupervised hierarchical clustering method was performed using Cluster 3.0 (30) with Pearson
1014 Correlation and average linkage rule. Gene expression data (FPKM of all samples) was taken and log2
1015 transformed. Low expressed (FPKM<0.05) and invariant genes were removed. Then genes were
1016 centered and clustering was performed based on differential expression pattern of genes and fold
1017 change. Finally, the heatmap was visualized in Java TreeView 3.0.

1018 Biological analysis of differentially expressed transcripts and pathway regulatory network modeling

1019 Statistically significant differentially expressed transcripts were subjected to GO and Pathway
1020 enrichment using DAVID tool. Only those GO and pathways with a FDR score of <=0.05 was considered
1021 for further downstream analysis. Key biologically dysregulated GO and Pathways along with the
1022 differentially expressed genes was provided as an input to Pathreg algorithm from Theomics
1023 International Pvt Ltd, Bangalore, India for gene regulatory network modeling. The result (nodes and
1024 edges) of the Pathreg algorithm was provided as an input to Cytoscape v2.8.2 to identify key nodes and
1025 edges that could be representative of the gene regulatory changes upon treatment.

1026 **Quantitative real time PCR:** Total RNA was isolated from the 3T3L1 cells and epididymal fat pads by
1027 phenol-chloroform method. In case of LTK-14A treatment, 3T3L1 cells were allowed to differentiate for
1028 7 days following the standard adipogenesis protocol, in presence of the compound at 25 µM
1029 concentration. The control experiments were 3T3L1 cells differentiated with or without DMSO as
1030 solvent control and differentiation was done only with the addition of only the cocktail of chemicals for
1031 adipogenesis. RNA was isolated from the cells after the period of 7 days in all three cases. For isolation
1032 of RNA from mice fat pads, the adiose tissue samples were lysed in Trizol using a mechanical
1033 homogenizer followed by phenol-chloroform method of extraction. The isolated RNA samples were
1034 treated with 2 units/µL DNase I to remove any residual DNA followed by ethanol precipitation at -80°C.
1035 2µg RNA was used for cDNA synthesis using MMLV reverse transcriptase (Sigma) in presence of 0.5 mM
1036 dNTP and 3.5 µM oligo dT (Sigma). RT-qPCR amplification was done in kappa SYBR green reagent
1037 (Biosystems) with the help of Real time PCR instrument (Applied Biosystems by Life Technologies).For
1038 estimation of relative fold change in RNA expression, the following calculation was done: Relative fold
1039 change = 2-ΔΔCt, where ΔΔCt=ΔCt value of sample – ΔCt value of control and ΔCt= Ct value of target – Ct
1040 value of internal control actin for individual sample. The sequences of primers are provided in Table 4.

1041 **Hematoxylin and eosin staining of liver and adipose tissues:** Staining was performed on paraffin
1042 embedded sections of liver and epididymal fat pads having the thickness of 5 µm and 10 µm
1043 respectively. Briefly, the sections were deparaffinized in xylene, followed by immersion in absolute
1044 alcohol, 90% ethanol, 70% ethanol, 50% ethanol and water before staining with hematoxylin for 5-10
1045 minutes. The sections were immersed in above mentioned solutions in reverse order before counter-

staining in eosin for 15 seconds. Then the samples were dipped in absolute ethanol and xylene before mounting with DPX.

MTT assay: 12500 cells/ml were seeded in presence/absence of LTK-14A in 96-well plate and at different intervals of time (2 days, 4 days, 6 days) , 1/10th volume of 5mg/ml MTT solution was added to it followed by incubation at 37 °C for 3 hours. The formed crystals were dissolved in DMSO and spectrometric estimation of colour intensity was done at 570 nm.

Evaluation of mutagenecity by plate incorporation assay: Five doses of LTK-14A (10.0□g, 33.0□g, 100.0□g, 333.0□g and 1000.0□g/plate) were selected to check for its possible mutagenecity. Seven groups decided as Group 1- Control, Group 2 Positive Control and 5 doses of LTK-14A (Group 3 to Group 7: 10.0□g, 33.0□g, 100.0□g, 333.0□g and 1000.0□g/plate) were tested. Four tester strains of Salmonella typhimurium (TE 97a, TA 98, TA 100, TA102) were used and their respective positive controls were used in absence of S9 fraction (Table 5); 2-aminoanthracene was used as the positive control in presence of S9 fraction (Table 5). The tester strains were grown overnight in Luria Broth antibiotic selection medium at 37□C. LTK-14A prepared in DMSO was mixed with the bacterial culture, 0.5mM Histidine-Biotin and top agar in a culture tube and the content was overlaid on to minimal glucose plate. In case of plate incorporation assay with S9 mix, LTK-14A was incubated with S9 mix in cold condition for 15 to 20 minutes followed by the same procedure as the plate incorporation assay without S9. The plates were incubated in an inverted position in 37□C incubators for 48 hours following which the number of revertants was counted using automated colony counter.

Single dose toxicity study: The single dose toxicity study on LTK-14A was conducted in accordance with Good Laboratory Practice Principles as published by the OECD in 1998, in accordance with the Drugs and Cosmetics Rule (New Drugs and Clinical trials, 2019/ DCGI). LTK-14A (formulated in vehicle i.e. 0.5% sodium salt of carboxymethyl cellulose) was administered to Sprague Dawley rats once by oral route on the day of scheduled treatment. The three treatment groups were 250 mg, 500 mg, and 1000 mg/kg body weight, while vehicle control was administered to control group. The rat equivalent doses were calculated from the dosage used in mice experiments following FDA guidelines for drug administration. The doses finally administered were 10, 20 and 40 times the corresponding mice equivalent dose. Food, but not water, was removed thus letting the animals fast over night prior to dosing. After administration of LTK-14A, food was withheld for further 2-3 hours and the animals were observed at 30 minutes, 1 hour, 2 hours and 4 hours from the time of dosing. Animals were subsequently observed once daily for any signs of toxicity, mortality, or any other observations including conditions of skin, hair coat, eyes, mucous membrane, movement, activity, tremors, convulsions, salivation, diarrhea, posture, piloerection and lethargy. Food intake, water intake and body weight of animals was recorded weekly. Terminal sacrifice of surviving animals was performed after 14 days using CO2 euthanasia technique following which animals were necropsied. Animals were fasted over night before necropsy. Gross observations were recorded.

Supplementary Figure 1

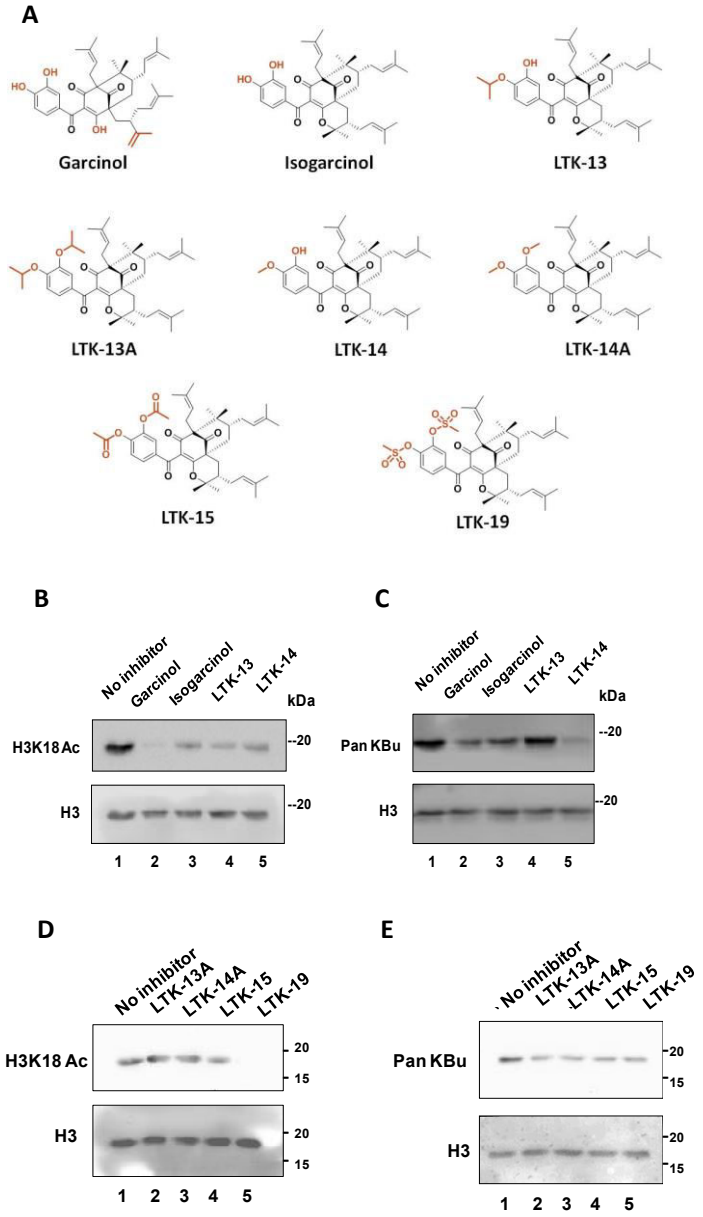

1084

1085

1086

1087

1088

1089

1090

1091 Sup.Fig.1: (A) Structures of garcinol and its cyclised and substituted derivatives. The site of internal
1092 cyclisation and mono/di-substitutions are shown in brown colour. Initial screening of the different
1093 monno-substituted derivatives for their differential effect on p300 catalysed acetylation (B) and
1094 butyrylation (C) of histone H3 at a concentration of 10 µM. Immunoblotting with antibodies against
1095 acetylated H3K18 (B) and pan-butyryl lysine (C). Similar screening was performed with di-substituted
1096 derivatives for their effect on p300 catalysed acetylation (D) and (E) of histone H3 at a concentration of
1097 25 µM.

1098

1099

1100

1101

1102

1103

1104

1105

1106

1107

1108

1109

1110

1111

1112

1113

1114

1115

1116

1117

1118

Supplementary Figure 2

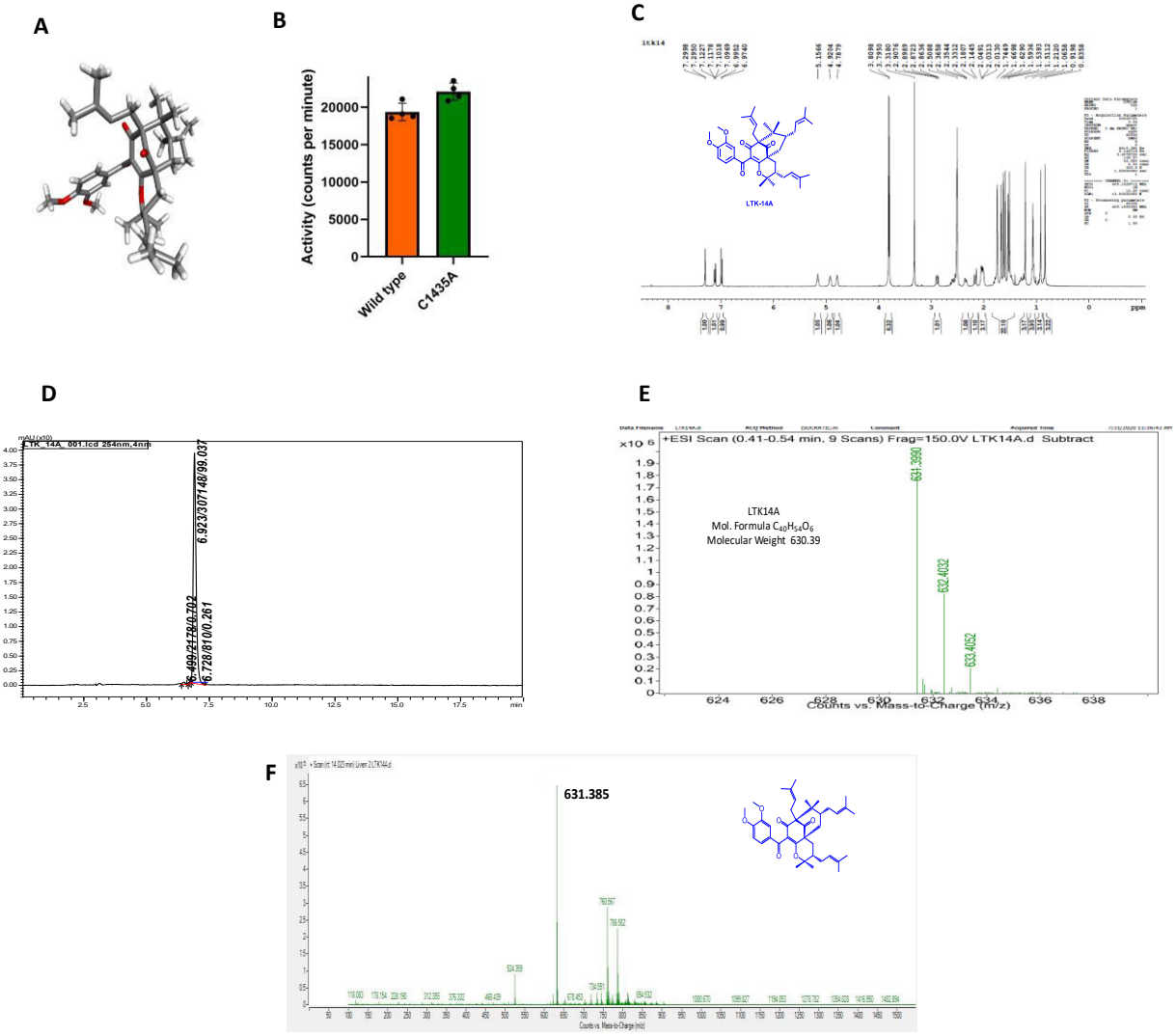

1119

1120

1121

1122

1123

1124

1125

1126

1127

Sup. Fig.2: (A) Crystal structure of LTK-14A (CCDC: 1969185) (B) Bar graphs depicting the acetyltransferase activity of wild type an mutant C1438A p300 catalytic domain as meeasured by filter binding assay. Error bars denote mean +/- SEM of four technical replicates; two-tailed unpaired Student's t-test: * $P < 0.05$, ** $P < 0.01$, *** $P < 0.001$, ns: not significant. (C) Proton NMR, (D) HR-MS spectra and (D) HPLC chromatogram of LTK-14A. (F) The presence of LTK-14A in the physiological system upon administering the compound was verified by LC-ESI-MS analysis of the metabolite extracts of liver.

Supplementary Figure 3

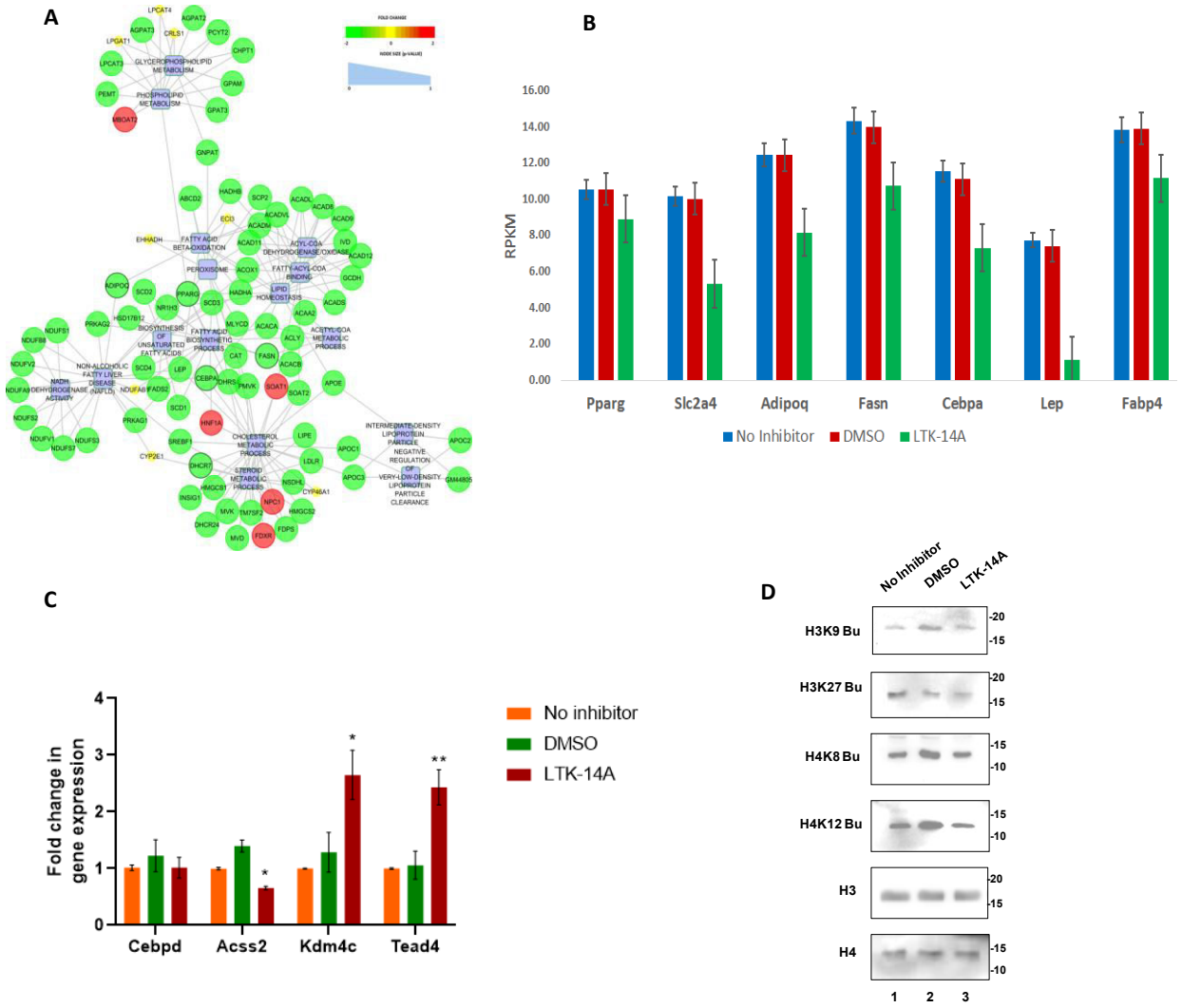

1156

1157

1158

1159

1160

1161

1162

1163 Sup. Fig. 3: (A) Molecular pathway analysis for the expression status of major lipid metabolism related
1164 genes and their interrelationship with the pathways that were affected in LTK-14A versus untreated
1165 conditions. (B) Pro-adipogenic genes that could be putative targets for LTK-14A were identified and
1166 RPKM values for these genes have been depicted graphically.(C) RT-qPCR analysis was performed to
1167 validate the putative target genes of LTK-14A. Error bars denote mean +/- SEM of three biological
1168 replicates. (D) Histone butyrylation levels in 3T3L1 cells that were treated with LTK-14A were compared
1169 with that in DMSO treated and untreated conditions by immunoblotting with antibodies against
1170 butyrylated histone H3K9, H3K27, H4K8 and H4K12. Histones H3 and H4 were used as loading controls.

1171

1172

1173

1174

1175

1176

1177

1178

1179

1180

1181

1182

1183

1184

1185

1186

1187

1188

1189

1190

Supplementary Figure 4

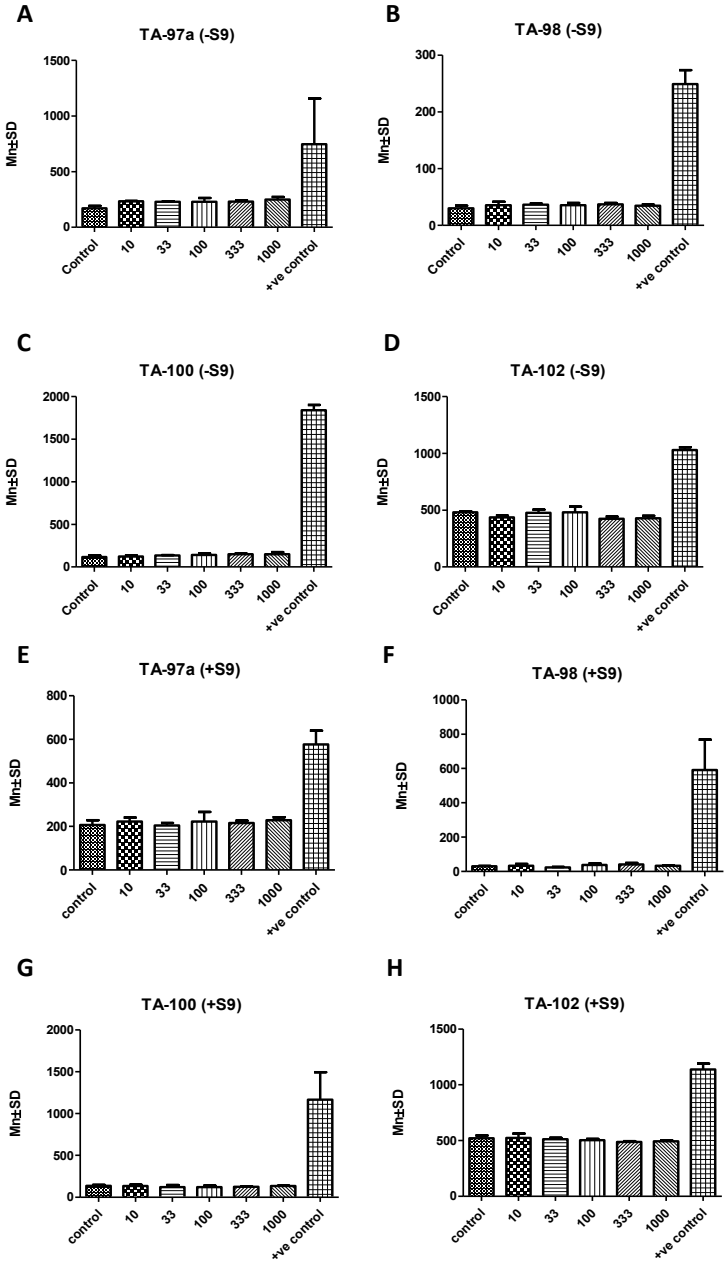

1191

1192

1193

1194

1195

1196

1197 Sup. Fig.4: Evaluation of mutagenecity of LTK-14A at different doses was tested by performing plate
1198 incorporation assay with four different tester strains of Salmonella typhimurium (TE 97a, TA 98, TA 100,
1199 TA102). Panel (A) to (D) – tests without S9 fraction. Panel (E) to (H) – tests with S9 fractions. Error bars
1200 denote mean +/- SEM of three biological replicates; One-way ANOVA followed by Neman-Keuls test.

1201

1202

1203

1204

1205

1206

1207

1208

1209

1210

1211

1212

1213

1214

1215

1216

1217

1218

1219

1220

1221

1222

1223

Table 1: Crystal data and structure refinement for LTK14A (CCDC: 1969185)

Empirical formula	$C_{40}H_{54}O_6$
Formula weight	630.86
Temperature/K	296 (2)
Crystal system	monoclinic
Space group	C2
a/Å	19.1677(11)
b/Å	11.5860(7)
c/Å	16.8399(11)
α/°	90
β/°	90
γ/°	90
Volume/$Å^3$	3739.8(4)
Z	110
ρ_{calc}g/cm^3	1.417
μ/mm^{-1}	0.131
F(000)	1650
Crystal size/mm^3	0.35 × 0.18 × 0.15
Radiation	MoKα (λ = 0.71073)
2Θ range for data collection/°	0.995 to 25.75
Index ranges	$-23 \leq h \leq 23$, $-14 \leq k \leq 14$, $-20 \leq l \leq 20$
Reflections collected	108274
Independent reflections	108274 [R_{int} = 0.0811, R_{sigma} = 0.0325]
Data/restraints/parameters	7123/3/415
Goodness-of-fit on F^2	1.045
Final R indexes [I>=2σ (I)]	R_1 = 0.1038, wR_2 = 0.2797
Final R indexes [all data]	R_1 = 0.1362, wR_2 = 0.3157

1230 **Table 2: Food consumption pattern of mice used in obesity studies**

Set A			
Type of diet	**Chow diet**	**High fat diet**	**High fat diet and LTK-14A**
Average food consumed per mice per day (gram)	8.0157	1.95547	2.04051
Standard error of mean	1.31838	0.23142	0.24589
Set B			
Type of mice	**db +/-**	**db/db and vehicle control**	**db/db and LTK-14A**
Average food consumed per week per mouse (gram)	25.8	37.8	34
Standard error of mean	1.04	1.64	2.08

1231

1232 **Table 3: List of primers used in ChIP-qRTPCR**

Gene	**Primer sequence 5' - > 3'**
Pparg Fwd	AGCTCGATGACCATAAGCCT
Pparg Rev	ATAGGCAGTGCATCAGCGAA
Lep Fwd	AGGTCATGTGGACAGCTTGG
Lep Rev	CGTCCAGCCTTGCTTTTTCC
Cebpd Fwd	CGCTTTTCAGCCTGGACAG
Cebpd Rev	TGGAGTCAATGTAGGCGCTG

1233

1234 Table 4: List of primers used in gene expression analysis by qRTPCR

Gene	**Primer sequence 5' - > 3'**
Actin Fwd	**CCACTGTCGAGTCGCGTCC**
Actin Rev	**GTCATCCATGGCGAACTGGTG**
Pparg Fwd	**TCCGTGATGGAAGACCACTC**
Pparg Rev	**CCCTTGCATCCTTCACAAGC**
Cebpd Fwd	**ATCGACTTCAGCGCCTACAT**
Cebpd Rev	**GCTTTGTGGTTGCTGTTGAA**
aP2 Fwd	**TCTCCAGTGAAAACTTCGAT**
aP2 Rev	**TTACGCTGATGATCAATGTT**
Slc2a4 Fwd	**ACGACGGACACTCCATCTGTTG**
Slc2a4 Rev	**GGAGACATAGCTCATGGCTGGAA**
Lep Fwd	**GAGCGGGATCAGGTTTTGTGGT**
Lep Rev	**TGTCACTCTTTCCCGGTCTCTTCA**

Adipoq Fwd	**CAGTGGATCTGACGACACCAA**
Adipoq Rev	**GAACAGGAGAGCTTGCAACAGT**
Cebpa Fwd	**TACCGAGTAGGGGGAGCAAA**
Cebpa Rev	**TCATTTTTCTCACGGGGCCA**
TEAD4 Fwd	**GCCACAGCCTTCCACAGTAA**
TEAD4 Rev	**AAGCTCCTTGCCAAAACCCT**
Kdm4c Fwd	**CAGTGCGGAACAAGTCTTCCAA**
Kdm4c Rev	**CAGATGTTTCTGCGCCGCT**
Fasn Fwd	**GGGTGTGAGTGGTTCAGAGG**
Fasn Rev	**AGGGCAATGCTTGGTCCTTT**
Acss2 Fwd	**TCGGAACTTGATGCGATGGG**
Acss2 Rev	**TTTCCCCAAAACTCCCGTGG**

1235

1236 **Table 5: List of mutagenic agents used as positive control in Ames test**

Tester Strains	Without S9	With S9
TA-97a	9-aminoacridine (50µg/plate)	2-aminoanthracene (5µg/plate)
TA-98	N-nitro-o-phenylene diamine (2.5µg/plate)	2-aminoanthracene (5µg/plate)
TA-100	Sodiumazide (5µg/plate)	2-aminoanthracene (5µg/plate)
TA-102	Mitomycin C (0.5µg/plate)	2-aminoanthracene (5µg/plate)

1237

1238

1239

1240

1241

1242

1243

1244

1245

1246 **Table 6: Details of single dose toxicity test**

1247 **Body weight (gram, mean +/- SD of animals in all groups**

Group	Male				Female			
		Initial	Mid	Final		Initial	Mid	Final
Vehicle control	Mean	174.75	217.38	232.13	Mean	152.21	169.81	171.5
	±SD	7.61	11.38	18.38	±SD	6.58	6.57	6.65
LTK-14A (250 mg/Kg bw)	Mean	171.94	216.62	244.21	Mean	151.99	174.54	176.35
	±SD	6.87	13.63	29.81	±SD	6.43	6.06	9.5
LTK-14A (500 mg/Kg bw)	Mean	176.3	229.75	243.14	Mean	153.32	176.55	175.8
	±SD	5.53	17.08	12.25	±SD	6.44	10.86	6.48
LTK-14A (1000 mg/Kg bw)	Mean	176.24	217.65	226.19	Mean	153.81	178.58	179.52
	±SD	7.51	12.31	23.57	±SD	7.29	7.46	8.45

1248

1249 **Average food intake (gram/day/animal) in each group**

Group	Male			Female		
	Initial	Middle	Final	Initial	Middle	Final
Vehicle control	20.38	20.24	21.24	17.84	15.65	15.95
LTK-14A (250 mg/Kg bw)	20.03	20.79	22.62	20	16.32	16.65
LTK-14A (500 mg/Kg bw)	20.99	21.14	23.29	18.22	18.13	17.09
LTK-14A (1000 mg/Kg bw)	20.76	20.74	19.95	18.17	17.82	16.97

1250

1251 **Average water intake (ml/day/animal) in each group**

Group	Male			Female		
	Initial	Middle	Final	Initial	Middle	Final
Vehicle control	32	30	34	25	21	26
LTK-14A (250 mg/Kg bw)	32	27	34	26	21	24
LTK-14A (500 mg/Kg bw)	36	33	40	25	23	26
LTK-14A (1000 mg/Kg bw)	34	31	38	26	22	32

1252

1253